# REPORT DOCUMENTATION PAGE

*Form Approved*
**OMB No. 0704-0188**



| 1. REPORT DATE *(DD-MM-YYYY)* | 2. REPORT TYPE | 3. DATES COVERED *(From - To)* |
|---|---|---|
| 03/01/2012 | Annual Progress/Status | 05/2010-05/2011 |

**4. TITLE AND SUBTITLE**
Strongly Interacting Fermi Gases in Two Dimensions

**5a. CONTRACT NUMBER**
NA

**5b. GRANT NUMBER**
N00014-10-1-0843

**5c. PROGRAM ELEMENT NUMBER**

**6. AUTHOR(S)**
Zwierlein, Martin W

**5d. PROJECT NUMBER**

**5e. TASK NUMBER**

**5f. WORK UNIT NUMBER**

**7. PERFORMING ORGANIZATION NAME(S) AND ADDRESS(ES)**
Massachusetts Institute of Technology
77 Massachusetts Avenue
Cambridge, MA 02139

**8. PERFORMING ORGANIZATION REPORT NUMBER**

**9. SPONSORING/MONITORING AGENCY NAME(S) AND ADDRESS(ES)**
Office of Naval Research
875 North Randolph Street
Arlington, VA 22203-1995

**10. SPONSOR/MONITOR'S ACRONYM(S)**
ONR BD025

**11. SPONSORING/MONITORING AGENCY REPORT NUMBER**

**12. DISTRIBUTION AVAILABILITY STATEMENT**
Approved for Public Release; distribution is unlimited.

**13. SUPPLEMENTARY NOTES**

**14. ABSTRACT**
In this project we aim to directly realize a model system of strongly correlated electrons moving in two dimensions using ultracold fermionic atoms stored in a sheet of light. The goal is to create high-temperature superfluids in two dimensions, to establish interferometry and magnetometry with these systems, and to study the phase diagram of two-dimensional Fermi gases with arbitrary interactions and spin imbalance. Fast rotation will mimic high magnetic fields and allow the approach to the Quantum Hall regime. The system shares traits with High-Tc materials, where super currents flow between stacks of weakly connected two dimensional planes.
This year has seen rather spectacular progress where transport of Fermions has been studied, in work that we published in Nature. Recently, we were able to study the evolution of fermion pairing from three to two dimensions.

**15. SUBJECT TERMS**
Ultracold Atoms, Fermi Gases, Strong Interactions, Lower Dimensions, Strongly Correlated Materials, Quantum Simulators, Superconductivity

| 16. SECURITY CLASSIFICATION OF: | | | 17. LIMITATION OF ABSTRACT | 18. NUMBER OF PAGES..... | 19a. NAME OF RESPONSIBLE PERSON |
|---|---|---|---|---|---|
| a. REPORT | b. ABSTRACT | c. THIS PAGE | SAR | | 19b. TELEPONE NUMBER (*Include area code)* |
| UU | UU | | | | |

**Young Investigator Program – Office of Naval Research**
**Martin W. Zwierlein, MIT**

## Progress 06/2010-05/2011

### Overview

Our group studies strongly interacting mixtures of fermionic atoms, atoms with half-integer spin. In these novel systems we can realize superfluids of fermion pairs and other paradigms of many-body physics. The goal is to improve our understanding of strongly correlated systems, such as high-temperature superconductors, colossal magnetoresistive materials and heavy fermions.

### 1. Universal Spin Transport in a Strongly Interacting Fermi Gas

Ariel Sommer, Mark Ku, Giacomo Roati, and Martin W. Zwierlein

Nature 472, 201-204 (2011)

Transport of fermions is central in many fields of physics. Electron transport runs modern technology, defining states of matter such as superconductors and insulators. Transport of electron spin, rather than of charge, is being explored as a new way to carry information. Neutrino transport energizes supernova explosions following the collapse of a dying star, and hydrodynamic transport of the quark-gluon plasma governed the expansion of the early Universe. However, our understanding of non-equilibrium dynamics in such strongly interacting fermionic matter is still limited. Ultracold gases of fermionic atoms realize a pristine model for such systems and can be studied in real time with the precision of atomic physics. It has been established that even above the superfluid transition such gases flow as an almost perfect fluid with very low viscosity when interactions are tuned to a scattering resonance. However, in this work we show that spin currents, as opposed to mass currents, are maximally damped, and that interactions can be strong enough to reverse spin currents, with opposite spin components reflecting off each other. We determine the spin drag coefficient, the spin diffusivity, and the spin susceptibility, as a function of temperature on resonance and show that they obey universal laws at high temperatures. At low temperatures, the spin diffusivity approaches a minimum value set by h/m, the quantum limit of diffusion, where h is Planck's constant and m the atomic mass. For repulsive interactions, our measurements appear to exclude a metastable ferromagnetic state.

This work was featured in a Physics Today article, June 2011, by Barbara Gross-Levi, as well as in a Nature News&Views article by John Thomas.

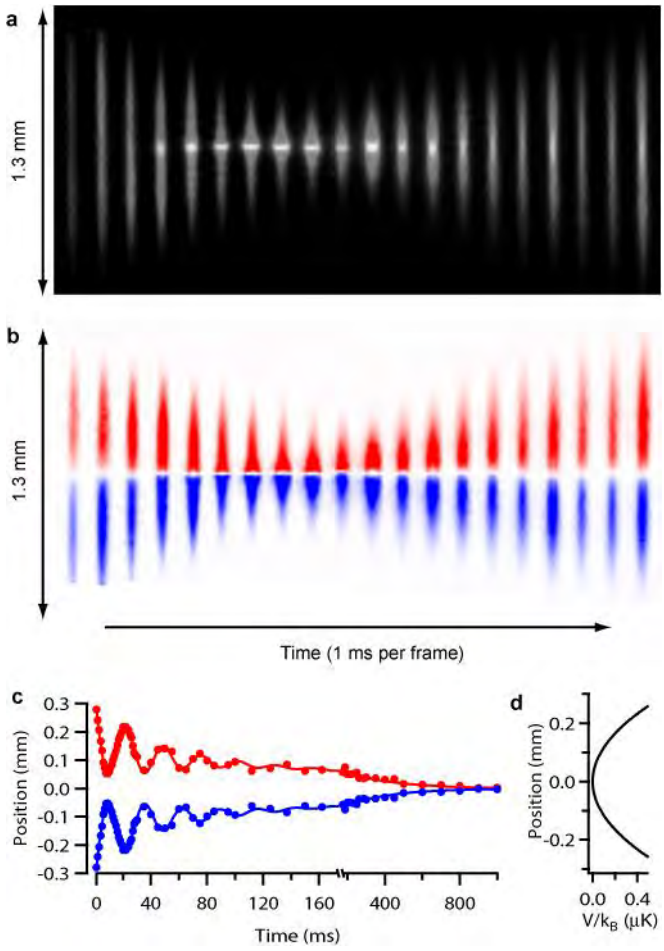


Figure 1 Observation spin reflection in a resonant collision between two oppositely spin-polarized clouds of fermions. a) shows the total column density and b) the difference in column densities of the two clouds (red: spin up, blue: spin down), after the magnetic field is set to the Feshbach resonance. The collision leads to the formation of a high-density interface between the two spin states. c) The separation between the centers of mass of the two spin states initially oscillates at a frequency of 1.63(2) nz, where nz = 22.8 Hz is the axial trap frequency. Even after half a second, there is still substantial spin separation. The diffusion time indicates a diffusivity on the order of h/m. d) Shows the harmonic trapping potential along the axis of symmetry.

## 2. Universal Spin Transport in Polaronic and Superfluid Fermi Gases

Ariel Sommer, Mark Ku, and Martin W. Zwierlein,

New Journal of Physics 13, 055009 (2011)

In this work, we present measurements of spin transport in ultracold gases of fermionic Lithium-6 in a mixture of two spin states at a Feshbach resonance. In particular, we study the spin-dipole mode, where the two spin components are displaced from each other against a harmonic restoring force. We prepare a highly imbalanced, or polaronic, spin mixture with a spin-dipole excitation and we observe strong, unitarity-limited damping of

the spin-dipole mode. In gases with small spin imbalance, below the Pauli limit for superfluidity, we observe strongly damped spin flow even in the presence of a superfluid core. This indicates strong mutual friction between superfluid and polarized normal spins, possibly involving Andreev reflection at the superfluid–normal interface.
This work was chosen as an IOP Select for the NJP Focus issue on Strongly Correlated Quantum Fluids: From Ultracold Quantum Gases to QCD Plasmas.

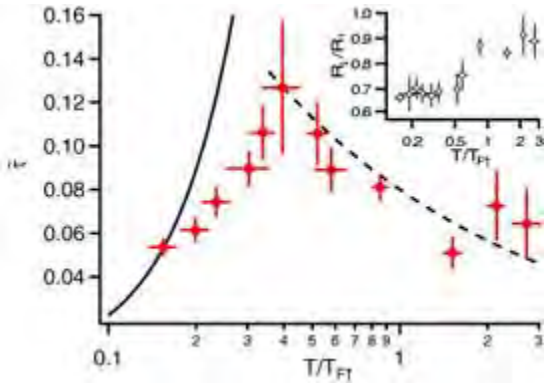


Figure 2 Spin Transport in Spin-Imbalanced, strongly interacting Fermi Gases. Shown is the relaxation time of the spin-dipole mode in a strongly interacting, trapped Fermi gas, as a function of the reduced temperature $T/T_{F,up}$, where $T_{F,up}$ is the Fermi energy of the majority spin up Fermi sea. At high temperatures, the classical prediction (dashed line) produces a good description of the data, whereas at low temperatures, Pauli pressure leads to a strong reduction of the relaxation time. The solid line is a prediction for the homogeneous gas.

### 3. Evolution of Fermion Pairing from Three to Two Dimensions

Ariel T. Sommer, Lawrence W. Cheuk, Mark Jen-Hao Ku, Waseem S. Bakr, Martin W. Zwierlein

Physical Review Letters, in print, preprint arXiv:1110.3058 (2011)

Interacting fermions in coupled two-dimensional (2D) layers present unique physical phenomena and are central to the description of unconventional superconductivity in high-transition-temperature cuprates and layered organic conductors. Reduced dimensionality enhances the effect of fluctuations, while interlayer coupling can stabilize superconductivity and even amplify the transition temperature. A fermionic superfluid loaded into a periodic potential should form stacks of two-dimensional superfluids with tunable interlayer coupling, a key ingredient of the model proposed by Anderson to explain high transition temperatures observed in the cuprates. For deep potentials in the regime of uncoupled 2D layers, increasing the temperature of the gas is expected to destroy superfluidity through the Berezinskii-Kosterlitz-Thouless mechanism, while more exotic multi-plane vortex loop excitations are predicted for a 3D-anisotropic BCS superfluid near the critical point.

In this work, we studied fermion pairing across the crossover from 3D to 2D in a periodic potential of increasing depth. We follow the evolution of fermion pairing in the dimensional crossover from 3D to 2D as a strongly interacting Fermi gas of $^6$Li atoms becomes confined to a stack of two-dimensional layers formed by a one-dimensional optical lattice. Decreasing the dimensionality leads to the opening of a gap in radiofrequency spectra, even on the BCS-side of a Feshbach resonance. With increasing lattice depth, the measured binding energy Eb of fermion pairs increases in surprising agreement with mean-field theory for the BEC-BCS crossover in two dimensions.

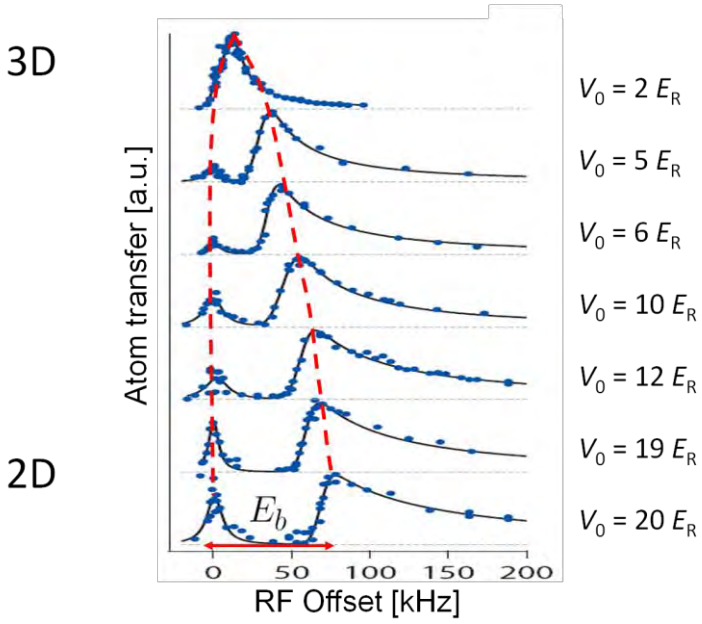


Figure 3 Evolution of Fermion Pairing from Three to Two Dimensions. Radio-Frequency Spectra show the opening of a pairing gap as the Fermi Gas is more and more confined to two dimensions. $V_0$ denotes the strength of the optical lattice used to confine the gas, in units of the recoil energy $E_R$ of a $^6$Li atom in the lattice.

## Publications

### Journal Articles

1. Cheng-Hsun Wu, Ibon Santiago, Jee Woo Park, Peyman Ahmadi, and Martin W. Zwierlein
   *Strongly Interacting Isotopic Bose-Fermi Mixture Immersed in a Fermi Sea*
   PRA **84**, 011601(R) (2011)

2. Ariel Sommer, Mark Ku, and Martin W. Zwierlein
   Spin Transport in Polaronic and Superfluid Fermi Gases

New J. Phys. 13, 055009 (2011)
IOP Select  Focus on Strongly Correlated Quantum Fluids

3. Ariel Sommer, Mark Ku, Giacomo Roati, and Martin W. Zwierlein
*Universal Spin Transport in a Strongly Interacting Fermi Gas*
Nature **472**, 201-204 (2011), arXiv:1101.0780 (2011)
See accompanying Nature News&Views by John Thomas
Physics Today  New Scientist  MIT News

4. Eric Vernier, David Pekker, Martin W. Zwierlein, and Eugene Demler
*Bound states of a localized magnetic impurity in a superfluid of paired ultracold fermions*
Phys. Rev. A 83, 033619 (2011)

5. D. Pekker, M. Babadi, R. Sensarma, N. Zinner, L. Pollet, M. W. Zwierlein, and E. Demler
Competition between pairing and ferromagnetic instabilities in ultracold Fermi gases near Feshbach resonances,
Phys. Rev. Lett. 106, 050402 (2011).

6. Ariel T. Sommer, Lawrence W. Cheuk, Mark Jen-Hao Ku, Waseem S. Bakr, Martin W. Zwierlein, 2011.
*Evolution of Fermion Pairing from Three to Two Dimensions*.
Phys. Rev. Lett., in print, arXiv:1110.3058.

**Invited Talks at Conferences**

1. *Universal Spin Transport in Strongly Interacting Fermi Gases.*
Nordita program "Quantum solids, liquids, and gases", Stockholm, Sweden, 8/11/2010
2. *Universal Spin Transport in Strongly Interacting Fermi Gases.*
KITP Conference "Frontiers of Ultracold Atoms and Molecules", Santa Barbara, CA, 10/11/2010
3. *Universal Spin Transport in Strongly Interacting Fermi Gases.*
Nordita conference "Frontiers of Condensed Matter Physics", Stockholm, Sweden, 1/6/2011
4. *Universal Spin Transport in Strongly Interacting Fermi Gases.*
ERATO Macroscopic Quantum Control Conference on Ultracold Atoms and Molecules, Tokyo, Japan, 1/24/2011
5. Universal Thermodynamics and Spin Transport in Strongly Interacting Fermi Gases.
APS March Meeting 2011, Dallas, Texas, 3/24/2011
6. Universal Thermodynamics and Spin Transport in Strongly Interacting Fermi Gases.
ESF-IFRAF Fermix meeting, Paris, France, 4/14/2011
7. *Strongly Interacting Isotopic Bose-Fermi Mixture Immersed in a Fermi Sea.*
3rd International Workshop on ultracold atoms/molecules
Hsinchu, Taiwan, 4/30/2011 (talk by C.-H. Wu)

8. *Universal Spin Transport in a Strongly Interacting Fermi Gas.*
   INT Symposium: Fermions from Cold Atoms to Neutron Stars: Benchmarking the Many-Body Problem, Seattle, WA, 5/18/2011
9. *Universal Thermodynamics across the Superfluid Transition in a Strongly Interacting Fermi Gas.*
   INT Symposium: Fermions from Cold Atoms to Neutron Stars: Benchmarking the Many-Body Problem, Seattle, WA, 5/18/2011
10. Universal Thermodynamics across the Superfluid Transition in a Strongly Interacting Fermi Gas.
    Workshop on Frontiers in Ultracold Fermi Gases, Trieste, Italy, 6/8/2011
11. Universal Thermodynamics and Spin Transport in Strongly Interacting Fermi Gases.
    Multiflavour strongly correlated quantum gases, Hamburg, Germany, 6/24/2011
12. Universal Thermodynamics and Spin Transport in Strongly Interacting Fermi Gases.
    International Conference on Quantum Technologies, Moscow, Russia, 7/14/2011
13. Universal Thermodynamics and Spin Transport in Strongly Interacting Fermi Gases.
    Non-standard superfluids and insulators, Trieste, Italy, 7/20/2011
14. *Universal Thermodynamics and Spin Transport in Strongly Interacting Fermi Gases.*
    Quantum phenomena in graphene, other low-dimensional materials, and optical lattices, Erice, Italy, 8/4/2011
15. *Universal Thermodynamics and Spin Transport in Strongly Interacting Fermi Gases.*
    Strongly Correlated Electron Systems (SCES 2011), Cambridge, UK, 9/2/2011
16. *Universal Thermodynamics and Spin Transport in Strongly Interacting Fermi Gases.*
    Frontiers in Quantum Gases (BEC2011). San Feliu, Spain, 9/13/2011
17. *Universal Thermodynamics and Spin Transport in Strongly Interacting Fermi Gases.*
    Cecam/Pauli-Center workshop "Modeling Materials With Cold Gases Through Simulations", Zurich, Switzerland, 11/10/2011
18. *Strongly Interacting Fermi Gases: Thermodynamics, Spin Transport, Dimensional Crossover.*
    NewSpin 2 workshop "Winter school and workshop on spin physics and topological effects in cold atoms, condensed matter, and beyond", College Station, TX, 12/16/2011

**Invited Talks at Colloquia and Seminars**

19. *Universal Spin Transport in Strongly Interacting Fermi Gases.*
    Atomic Physics Seminar, Cambridge, UK, 10/22/2010
20. Universal Thermodynamics and Spin Transport in Strongly Interacting Fermi Gases.
    Nuclear and Particle Theory Seminar, MIT Center for Theoretical Physics, Cambridge, MA, 2/14/2011
21. *A Little Big Bang: Ultracold Fermi Gases at the Quantum Limit.*
    Physics Colloquium, Colby College, Colby College, ME, 10/27/2011
22. *A Little Big Bang: Ultracold Fermi Gases at the Quantum Limit.*
    Physics Colloquium, University of Massachusetts, Boston, Boston, MA, 10/29/2011
23. *A Little Big Bang: Ultracold Fermi Gases at the Quantum Limit.*
    Physics Colloquium, Boston College, Boston, MA, 11/2/2011
24. *A Little Big Bang: Ultracold Fermi Gases with Strong Interactions.*
    Physics Colloquium, Yale University, New Haven, CT, 12/5/2011

**Contributed Talks by Group Members at Conferences**

25. Triply degenerate quantum mixture of 41K, 40K and 6Li.
    APS March Meeting 2011, Dallas, Texas, 3/23/2011
26. H4.00002: Revealing the superfluid phase transition in strongly interacting Fermi gases in a precision measurement of the equation of state.
    DAMOP 2011, Atlanta, Georgia, 6/15/2011
27. N5.00001 : Universal Spin Transport in Strongly Interacting Fermi Gases.
    DAMOP 2011, Atlanta, Georgia, 6/16/2011
28. P1.00007: Many body effects in a widely tunable Bose-Fermi mixture.
    DAMOP 2011, Atlanta, Georgia, 6/16/2011
29. P1.00003: Triply degenerate quantum mixture of 41K, 40K and 6Li.
    DAMOP 2011, Atlanta, Georgia, 6/16/2011
30. Universal Thermodynamics across the Superfluid Transition in a Strongly Interacting Fermi Gas.
    19th Particles & Nuclei International Conference (PANIC 2011), Cambridge, MA, 7/24/2011
31. Universal Spin Transport in a Strongly Interacting Fermi Gas.
    19th Particles & Nuclei International Conference (PANIC 2011), Cambridge, MA, 7/24/2011

## Honors and Awards

Martin Zwierlein:

- Young Investigator Award, Office of Naval Research, 2010
- Young Faculty Award, Defense Advanced Research Projects Agency, 2010
- Presidential Early Career Award for Scientists and Engineers, Office of Science and Technology Policy Executive Office of the President, 2010
- Silverman Family Career Development Chair, 2011 - current

A. Sommer received the Martin Deutsch Prize for Excellence in Experimental Physics from the MIT Physics Department

**Young Investigator Program – Office of Naval Research**
**Martin W. Zwierlein, MIT**

## Progress 06/2010-05/2011

### Overview

Our group studies strongly interacting mixtures of fermionic atoms, atoms with half-integer spin. In these novel systems we can realize superfluids of fermion pairs and other paradigms of many-body physics. The goal is to improve our understanding of strongly correlated systems, such as high-temperature superconductors, colossal magnetoresistive materials and heavy fermions.

### 1. Universal Spin Transport in a Strongly Interacting Fermi Gas

Ariel Sommer, Mark Ku, Giacomo Roati, and Martin W. Zwierlein

Nature 472, 201-204 (2011)

Transport of fermions is central in many fields of physics. Electron transport runs modern technology, defining states of matter such as superconductors and insulators. Transport of electron spin, rather than of charge, is being explored as a new way to carry information. Neutrino transport energizes supernova explosions following the collapse of a dying star, and hydrodynamic transport of the quark-gluon plasma governed the expansion of the early Universe. However, our understanding of non-equilibrium dynamics in such strongly interacting fermionic matter is still limited. Ultracold gases of fermionic atoms realize a pristine model for such systems and can be studied in real time with the precision of atomic physics. It has been established that even above the superfluid transition such gases flow as an almost perfect fluid with very low viscosity when interactions are tuned to a scattering resonance. However, in this work we show that spin currents, as opposed to mass currents, are maximally damped, and that interactions can be strong enough to reverse spin currents, with opposite spin components reflecting off each other. We determine the spin drag coefficient, the spin diffusivity, and the spin susceptibility, as a function of temperature on resonance and show that they obey universal laws at high temperatures. At low temperatures, the spin diffusivity approaches a minimum value set by h/m, the quantum limit of diffusion, where h is Planck's constant and m the atomic mass. For repulsive interactions, our measurements appear to exclude a metastable ferromagnetic state.

This work was featured in a Physics Today article, June 2011, by Barbara Gross-Levi, as well as in a Nature News&Views article by John Thomas.

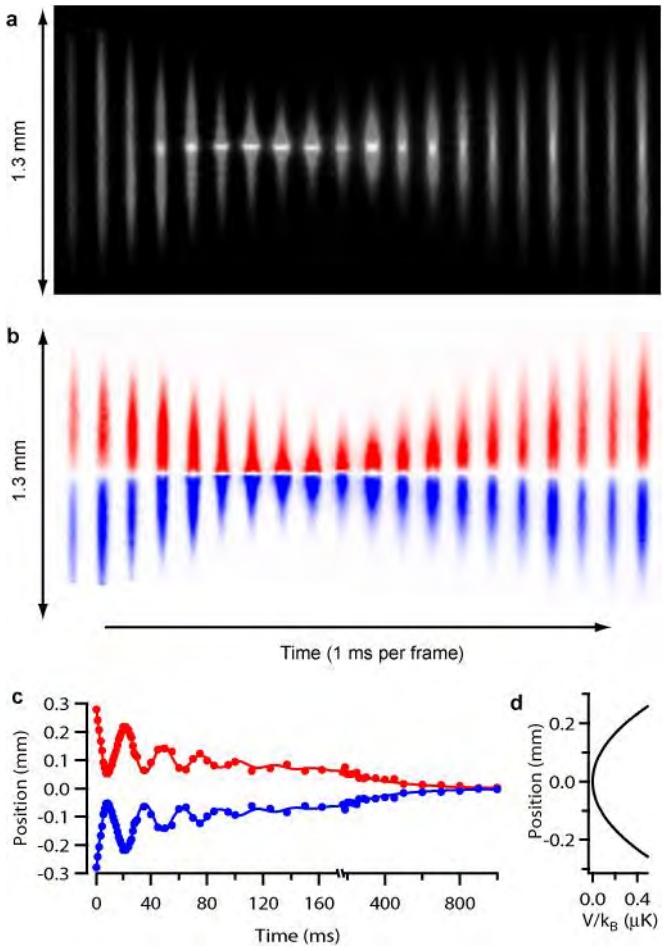


Figure 1 Observation spin reflection in a resonant collision between two oppositely spin-polarized clouds of fermions. a) shows the total column density and b) the difference in column densities of the two clouds (red: spin up, blue: spin down), after the magnetic field is set to the Feshbach resonance. The collision leads to the formation of a high-density interface between the two spin states. c) The separation between the centers of mass of the two spin states initially oscillates at a frequency of 1.63(2) nz, where nz = 22.8 Hz is the axial trap frequency. Even after half a second, there is still substantial spin separation. The diffusion time indicates a diffusivity on the order of h/m. d) Shows the harmonic trapping potential along the axis of symmetry.

## 2. Universal Spin Transport in Polaronic and Superfluid Fermi Gases

Ariel Sommer, Mark Ku, and Martin W. Zwierlein,

New Journal of Physics 13, 055009 (2011)

In this work, we present measurements of spin transport in ultracold gases of fermionic Lithium-6 in a mixture of two spin states at a Feshbach resonance. In particular, we study the spin-dipole mode, where the two spin components are displaced from each other against a harmonic restoring force. We prepare a highly imbalanced, or polaronic, spin mixture with a spin-dipole excitation and we observe strong, unitarity-limited damping of

the spin-dipole mode. In gases with small spin imbalance, below the Pauli limit for superfluidity, we observe strongly damped spin flow even in the presence of a superfluid core. This indicates strong mutual friction between superfluid and polarized normal spins, possibly involving Andreev reflection at the superfluid–normal interface.
This work was chosen as an IOP Select for the NJP Focus issue on Strongly Correlated Quantum Fluids: From Ultracold Quantum Gases to QCD Plasmas.

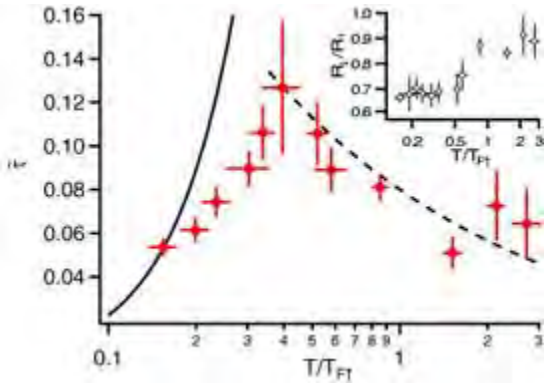


Figure 2 Spin Transport in Spin-Imbalanced, strongly interacting Fermi Gases. Shown is the relaxation time of the spin-dipole mode in a strongly interacting, trapped Fermi gas, as a function of the reduced temperature $T/T_{F,up}$, where $T_{F,up}$ is the Fermi energy of the majority spin up Fermi sea. At high temperatures, the classical prediction (dashed line) produces a good description of the data, whereas at low temperatures, Pauli pressure leads to a strong reduction of the relaxation time. The solid line is a prediction for the homogeneous gas.

### 3. Evolution of Fermion Pairing from Three to Two Dimensions

Ariel T. Sommer, Lawrence W. Cheuk, Mark Jen-Hao Ku, Waseem S. Bakr, Martin W. Zwierlein

Physical Review Letters, in print, preprint arXiv:1110.3058 (2011)

Interacting fermions in coupled two-dimensional (2D) layers present unique physical phenomena and are central to the description of unconventional superconductivity in high-transition-temperature cuprates and layered organic conductors. Reduced dimensionality enhances the effect of fluctuations, while interlayer coupling can stabilize superconductivity and even amplify the transition temperature. A fermionic superfluid loaded into a periodic potential should form stacks of two-dimensional superfluids with tunable interlayer coupling, a key ingredient of the model proposed by Anderson to explain high transition temperatures observed in the cuprates. For deep potentials in the regime of uncoupled 2D layers, increasing the temperature of the gas is expected to destroy superfluidity through the Berezinskii-Kosterlitz-Thouless mechanism, while more exotic multi-plane vortex loop excitations are predicted for a 3D-anisotropic BCS superfluid near the critical point.

In this work, we studied fermion pairing across the crossover from 3D to 2D in a periodic potential of increasing depth. We follow the evolution of fermion pairing in the dimensional crossover from 3D to 2D as a strongly interacting Fermi gas of $^6$Li atoms becomes confined to a stack of two-dimensional layers formed by a one-dimensional optical lattice. Decreasing the dimensionality leads to the opening of a gap in radiofrequency spectra, even on the BCS-side of a Feshbach resonance. With increasing lattice depth, the measured binding energy Eb of fermion pairs increases in surprising agreement with mean-field theory for the BEC-BCS crossover in two dimensions.

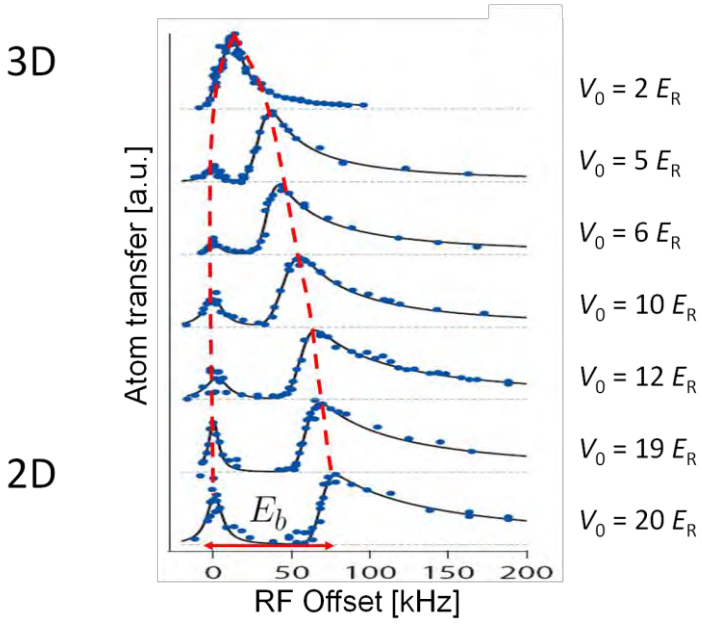


Figure 3 Evolution of Fermion Pairing from Three to Two Dimensions. Radio-Frequency Spectra show the opening of a pairing gap as the Fermi Gas is more and more confined to two dimensions. $V_0$ denotes the strength of the optical lattice used to confine the gas, in units of the recoil energy $E_R$ of a $^6$Li atom in the lattice.

## Publications

### Journal Articles

1. Cheng-Hsun Wu, Ibon Santiago, Jee Woo Park, Peyman Ahmadi, and Martin W. Zwierlein
   *Strongly Interacting Isotopic Bose-Fermi Mixture Immersed in a Fermi Sea*
   PRA **84**, 011601(R) (2011)

2. Ariel Sommer, Mark Ku, and Martin W. Zwierlein
   Spin Transport in Polaronic and Superfluid Fermi Gases

New J. Phys. 13, 055009 (2011)
IOP Select  Focus on Strongly Correlated Quantum Fluids

3. Ariel Sommer, Mark Ku, Giacomo Roati, and Martin W. Zwierlein
*Universal Spin Transport in a Strongly Interacting Fermi Gas*
Nature **472**, 201-204 (2011), arXiv:1101.0780 (2011)
See accompanying Nature News&Views by John Thomas
Physics Today  New Scientist  MIT News

4. Eric Vernier, David Pekker, Martin W. Zwierlein, and Eugene Demler
*Bound states of a localized magnetic impurity in a superfluid of paired ultracold fermions*
Phys. Rev. A 83, 033619 (2011)

5. D. Pekker, M. Babadi, R. Sensarma, N. Zinner, L. Pollet, M. W. Zwierlein, and E. Demler
Competition between pairing and ferromagnetic instabilities in ultracold Fermi gases near Feshbach resonances,
Phys. Rev. Lett. 106, 050402 (2011).

6. Ariel T. Sommer, Lawrence W. Cheuk, Mark Jen-Hao Ku, Waseem S. Bakr, Martin W. Zwierlein, 2011.
*Evolution of Fermion Pairing from Three to Two Dimensions*.
Phys. Rev. Lett., in print, arXiv:1110.3058.

**Invited Talks at Conferences**

1. *Universal Spin Transport in Strongly Interacting Fermi Gases.*
Nordita program "Quantum solids, liquids, and gases", Stockholm, Sweden, 8/11/2010
2. *Universal Spin Transport in Strongly Interacting Fermi Gases.*
KITP Conference "Frontiers of Ultracold Atoms and Molecules", Santa Barbara, CA, 10/11/2010
3. *Universal Spin Transport in Strongly Interacting Fermi Gases.*
Nordita conference "Frontiers of Condensed Matter Physics", Stockholm, Sweden, 1/6/2011
4. *Universal Spin Transport in Strongly Interacting Fermi Gases.*
ERATO Macroscopic Quantum Control Conference on Ultracold Atoms and Molecules, Tokyo, Japan, 1/24/2011
5. Universal Thermodynamics and Spin Transport in Strongly Interacting Fermi Gases.
APS March Meeting 2011, Dallas, Texas, 3/24/2011
6. Universal Thermodynamics and Spin Transport in Strongly Interacting Fermi Gases.
ESF-IFRAF Fermix meeting, Paris, France, 4/14/2011
7. *Strongly Interacting Isotopic Bose-Fermi Mixture Immersed in a Fermi Sea.*
3rd International Workshop on ultracold atoms/molecules
Hsinchu, Taiwan, 4/30/2011 (talk by C.-H. Wu)

8. *Universal Spin Transport in a Strongly Interacting Fermi Gas.*
   INT Symposium: Fermions from Cold Atoms to Neutron Stars: Benchmarking the Many-Body Problem, Seattle, WA, 5/18/2011
9. *Universal Thermodynamics across the Superfluid Transition in a Strongly Interacting Fermi Gas.*
   INT Symposium: Fermions from Cold Atoms to Neutron Stars: Benchmarking the Many-Body Problem, Seattle, WA, 5/18/2011
10. Universal Thermodynamics across the Superfluid Transition in a Strongly Interacting Fermi Gas.
    Workshop on Frontiers in Ultracold Fermi Gases, Trieste, Italy, 6/8/2011
11. Universal Thermodynamics and Spin Transport in Strongly Interacting Fermi Gases.
    Multiflavour strongly correlated quantum gases, Hamburg, Germany, 6/24/2011
12. Universal Thermodynamics and Spin Transport in Strongly Interacting Fermi Gases.
    International Conference on Quantum Technologies, Moscow, Russia, 7/14/2011
13. Universal Thermodynamics and Spin Transport in Strongly Interacting Fermi Gases.
    Non-standard superfluids and insulators, Trieste, Italy, 7/20/2011
14. *Universal Thermodynamics and Spin Transport in Strongly Interacting Fermi Gases.*
    Quantum phenomena in graphene, other low-dimensional materials, and optical lattices, Erice, Italy, 8/4/2011
15. *Universal Thermodynamics and Spin Transport in Strongly Interacting Fermi Gases.*
    Strongly Correlated Electron Systems (SCES 2011), Cambridge, UK, 9/2/2011
16. *Universal Thermodynamics and Spin Transport in Strongly Interacting Fermi Gases.*
    Frontiers in Quantum Gases (BEC2011). San Feliu, Spain, 9/13/2011
17. *Universal Thermodynamics and Spin Transport in Strongly Interacting Fermi Gases.*
    Cecam/Pauli-Center workshop "Modeling Materials With Cold Gases Through Simulations", Zurich, Switzerland, 11/10/2011
18. *Strongly Interacting Fermi Gases: Thermodynamics, Spin Transport, Dimensional Crossover.*
    NewSpin 2 workshop "Winter school and workshop on spin physics and topological effects in cold atoms, condensed matter, and beyond", College Station, TX, 12/16/2011

**Invited Talks at Colloquia and Seminars**

19. *Universal Spin Transport in Strongly Interacting Fermi Gases.*
    Atomic Physics Seminar, Cambridge, UK, 10/22/2010
20. Universal Thermodynamics and Spin Transport in Strongly Interacting Fermi Gases.
    Nuclear and Particle Theory Seminar, MIT Center for Theoretical Physics, Cambridge, MA, 2/14/2011
21. *A Little Big Bang: Ultracold Fermi Gases at the Quantum Limit.*
    Physics Colloquium, Colby College, Colby College, ME, 10/27/2011
22. *A Little Big Bang: Ultracold Fermi Gases at the Quantum Limit.*
    Physics Colloquium, University of Massachusetts, Boston, Boston, MA, 10/29/2011
23. *A Little Big Bang: Ultracold Fermi Gases at the Quantum Limit.*
    Physics Colloquium, Boston College, Boston, MA, 11/2/2011
24. *A Little Big Bang: Ultracold Fermi Gases with Strong Interactions.*
    Physics Colloquium, Yale University, New Haven, CT, 12/5/2011

**Contributed Talks by Group Members at Conferences**

25. Triply degenerate quantum mixture of 41K, 40K and 6Li.
    APS March Meeting 2011, Dallas, Texas, 3/23/2011
26. H4.00002: Revealing the superfluid phase transition in strongly interacting Fermi gases in a precision measurement of the equation of state.
    DAMOP 2011, Atlanta, Georgia, 6/15/2011
27. N5.00001 : Universal Spin Transport in Strongly Interacting Fermi Gases.
    DAMOP 2011, Atlanta, Georgia, 6/16/2011
28. P1.00007: Many body effects in a widely tunable Bose-Fermi mixture.
    DAMOP 2011, Atlanta, Georgia, 6/16/2011
29. P1.00003: Triply degenerate quantum mixture of 41K, 40K and 6Li.
    DAMOP 2011, Atlanta, Georgia, 6/16/2011
30. Universal Thermodynamics across the Superfluid Transition in a Strongly Interacting Fermi Gas.
    19th Particles & Nuclei International Conference (PANIC 2011), Cambridge, MA, 7/24/2011
31. Universal Spin Transport in a Strongly Interacting Fermi Gas.
    19th Particles & Nuclei International Conference (PANIC 2011), Cambridge, MA, 7/24/2011

## Honors and Awards

Martin Zwierlein:

- Young Investigator Award, Office of Naval Research, 2010
- Young Faculty Award, Defense Advanced Research Projects Agency, 2010
- Presidential Early Career Award for Scientists and Engineers, Office of Science and Technology Policy Executive Office of the President, 2010
- Silverman Family Career Development Chair, 2011 - current

A. Sommer received the Martin Deutsch Prize for Excellence in Experimental Physics from the MIT Physics Department

Spin transport in polaronic and superfluid Fermi gases



2011 New J. Phys. 13 055009

(http://iopscience.iop.org/1367-2630/13/5/055009)

New Journal of Physics
The open-access journal for physics

# Spin transport in polaronic and superfluid Fermi gases

**Ariel Sommer**[1], **Mark Ku and Martin W Zwierlein**
Department of Physics, MIT-Harvard Center for Ultracold Atoms, MIT, Cambridge, MA 02139, USA
and
Research Laboratory of Electronics, MIT, Cambridge, MA 02139, USA
E-mail: atsommer@mit.edu

*New Journal of Physics* **13** (2011) 055009 (14pp)
Received 10 February 2011
Published 24 May 2011
Online at http://www.njp.org/
doi:10.1088/1367-2630/13/5/055009

**Abstract.** We present measurements of spin transport in ultracold gases of fermionic $^6$Li in a mixture of two spin states at a Feshbach resonance. In particular, we study the spin-dipole mode, where the two spin components are displaced from each other against a harmonic restoring force. We prepare a highly imbalanced, or polaronic, spin mixture with a spin-dipole excitation and we observe strong, unitarity-limited damping of the spin-dipole mode. In gases with small spin imbalance, below the Pauli limit for superfluidity, we observe strongly damped spin flow even in the presence of a superfluid core. This indicates strong mutual friction between superfluid and polarized normal spins, possibly involving Andreev reflection at the superfluid–normal interface.

**Contents**



[1] Author to whom any correspondence should be addressed.

## 1. Introduction

The quality of transport is one of the most important properties distinguishing states of matter. Of great technical importance, electrons in condensed matter materials can flow as currents or supercurrents, or be localized in an insulator, or even switch their state of conductivity through controllable parameters like an applied magnetic field. It is the task of many-body physics to develop models that may explain the observed transport properties in a system. Dilute atomic gases cooled to quantum degeneracy provide ideal systems for testing many-body theories. In particular, Feshbach resonances [1] in atomic Fermi gases allow experimental control over the strength of two-body interactions, giving access to the Bose–Einstein condensation to Bardeen–Cooper–Schrieffer superfluid (BEC–BCS) crossover regime [2, 3]. Transport properties have played an important role in characterizing strongly interacting Fermi gases in the BEC-BCS crossover, with the observation of hydrodynamic flow indicating nearly perfect fluidity [4, 5], the measurement of collective excitation frequencies probing the equation of state [6–8], and the observation of vortex lattices in rotating gases demonstrating superfluidity [9]. The first observations of spin transport in Fermi gases were obtained in the weakly interacting regime, and showed the onset of Pauli blocking of collisions [10], and the transition from collisionless to hydrodynamic behavior [11]. Spin excitations have also been observed in Fermi gases as long-lived spin waves near zero scattering length [12].

Here we study spin transport in strongly interacting two-component Fermi gases. Spin currents are strongly damped in such systems due to the high collision rate between opposite spin atoms: as two-body scattering does not conserve relative momentum, each scattering event on average reduces the net spin current [13]. At the Feshbach resonance, scattering is maximal, with a mean-free path between collisions of opposite spins that can be as short as one interparticle spacing—the smallest possible in a three-dimensional (3D) gas. Measurements of spin transport in strongly interacting Fermi gases with an equal number of atoms in two spin states were recently reported [14]. Interactions were shown to be strong enough to reverse spin currents, with two clouds of opposite spin almost perfectly repelling each other. The spin diffusivity was found to reach a lower limit of the order of $\hbar/m$ at unitarity, the quantum limit of diffusion. Here, we consider the case where the number of atoms in the two states is unequal, and study spin transport in the polaron and phase-separated superfluid regimes. In highly polarized systems that remain non-superfluid down to zero temperature [15–17], spin currents are expected to become undamped due to Pauli blocking [18–20]. In this imbalanced regime, a high-frequency mode observed after a compressional excitation was interpreted as a weakly damped spin quadrupole (or breathing) mode [21]. The question of the damping properties of the spin excitation and its temperature dependence was left open. Spin transport properties of ultracold Fermi gases have been investigated theoretically most recently in [18–20], [22–24], allowing comparison between theory and experiment.

In section 2, we present measurements of the damping rate of spin excitations in highly polarized Fermi gases as a function of temperature. We show that damping is maximal at finite temperatures. In section 3, we study smaller spin polarizations, below the Pauli limit of superfluidity [15], just enough to reveal the presence of a superfluid core in the system. We show that the spin-dipole mode is strongly damped in the presence of the superfluid. In a partially polarized Fermi gas, damping of spin motion is expected to persist at low temperatures due to Andreev reflection [20].

## 2. Highly imbalanced Fermi gases

Fermi gases with resonant interactions can remain normal down to zero temperature if the spin imbalance exceeds the Pauli (or the Clogston–Chandrasekhar) limit [15, 16, 21, 25, 26, 39]. We refer to the spin state with the larger population of atoms as the majority, or spin-up state, and the state with fewer atoms as the minority, or spin-down state. Radio-frequency (RF) spectroscopy [17] on such systems confirms the quasi-particle picture [27–29] where minority atoms are dressed by the majority Fermi sea, forming a quasi-particle known as the Fermi polaron. The energy of a single polaron in a zero-temperature Fermi sea of spin-up atoms has been described using the effective Hamiltonian [18, 19, 30],

$$H = -\alpha\mu_\uparrow + \frac{\mathbf{p}^2}{2m^*}, \tag{1}$$

where $\mathbf{p}$ is the momentum of the polaron, $m^*$ is the polaron effective mass, $\mu_\uparrow$ is the local spin-up chemical potential and $\alpha$ characterizes the polaron binding energy. The parameters $\alpha$ and $m^*/m$, where $m$ is the bare mass of spin-up and spin-down fermions, have been measured experimentally [17, 21, 31, 32] and calculated theoretically [30], [33–35], giving $\alpha = 0.62$ and $m^*/m \approx 1.2$ at zero temperature.

We consider a mixture of $N_\uparrow$ spin-up fermions and $N_\downarrow$ spin-down fermions at temperature $T$ with equal masses and resonant interactions, held in a spin-independent potential of the form

$$V(\rho, z) = \tfrac{1}{2}m\omega_z^2 z^2 + V_\rho(\rho), \tag{2}$$

where $\rho^2 = x^2 + y^2$. The spin-up (down) clouds have density $n_{\uparrow(\downarrow)}(\mathbf{r})$ at position $\mathbf{r}$. The minority cloud is initially displaced by a small amount $Z_\downarrow(0)$ along the $z$-axis and is allowed to relax to its equilibrium position.

In the limit $N_\downarrow \ll N_\uparrow$, the motion of the spin-up cloud due to momentum absorbed from the spin-down cloud may be neglected. The equation of motion of the spin-down center of mass $Z_\downarrow$ is then [18]

$$m^*\ddot{Z}_\downarrow + (1+\alpha)m\omega_z^2 Z_\downarrow + \frac{m^*}{N_\downarrow}\int \mathrm{d}^3 r\, n_\downarrow(\mathbf{r})\frac{v_\downarrow(\mathbf{r})}{\tau_P(\mathbf{r})} = 0, \tag{3}$$

where the factor of $(1+\alpha)$ is due to the attraction of the minority fermions to the majority cloud, $1/\tau_P$ is the local momentum relaxation rate due to collisions [18] and is equivalent to the spin drag coefficient [13, 22], and $v_\downarrow$ is the local drift velocity of spin-down atoms. By dimensional analysis, $\hbar/\tau_P(\mathbf{r})$ must be given by the local majority Fermi energy times a universal dimensionless function of the local reduced temperature $T/T_{\mathrm{F}\uparrow}^{\mathrm{local}}(\mathbf{r})$ and the local ratio $T_{\mathrm{F}\downarrow}^{\mathrm{local}}(\mathbf{r})/T_{\mathrm{F}\uparrow}^{\mathrm{local}}(\mathbf{r})$ of the Fermi temperatures, where $T_{\mathrm{F}\uparrow(\downarrow)}^{\mathrm{local}}(\mathbf{r})$ is the local majority (minority) Fermi temperature. The first two terms in (3) follow from (1), (2) and the local density approximation, while the third term is due to damping and is not captured in (1). Equation (3) neglects a possible back-action of the minority on the majority atoms that might deform the majority density profile.

In our experimental realization of this transport problem, we use a gas of ultracold fermionic $^6$Li atoms. The $^6$Li atoms are cooled sympathetically with $^{23}$Na [36] and loaded into a hybrid optical and magnetic trap with an adjustable bias magnetic field [37]. The magnetic field curvature provides essentially perfect harmonic confinement along the axial ($z$) direction, while the optical dipole trap (laser wavelength 1064 nm, waist 115 $\mu$m) provides trapping in the radial

directions, with negligible contribution to the axial confinement. With this system, we perform a collection of time series measurements. In each time series, we prepare the system in a chosen initial state and observe its evolution.

At the Feshbach resonance at 834 G, the magnetic moments of 'spin-up' and 'spin-down' atoms, the two lowest hyperfine states of $^6$Li, are equal to 1 part in 1000, since their electron spin is in fact aligned with the magnetic field. Inducing a spin current is therefore extremely challenging on resonance. However, at lower fields, their magnetic moments differ, allowing separation of the two gas clouds by a magnetic field gradient. Our experimental procedure for producing these separated clouds is as follows.

We prepare the system starting with about $1 \times 10^7$ atoms of $^6$Li in the lowest hyperfine state, at a total magnetic field of 300 G. A small fraction of atoms are transferred to the second-lowest hyperfine state using a RF Landau–Zener sweep. The mixture is then evaporatively cooled for a variable amount of time by lowering the depth of the optical dipole trap from $k_B \times 7\,\mu$K to a variable final depth between $k_B \times 0.5\,\mu$K and $k_B \times 1\,\mu$K, where $k_B$ is the Boltzmann constant. The optical dipole trap depth is then raised to $k_B \times 6\,\mu$K, where the zero-temperature Fermi energy in the majority state is between $k_B \times 0.8\,\mu$K and $k_B \times 1.3\,\mu$K.

After the spin mixture is prepared at 300 G, the total magnetic field is reduced gradually over 500 ms to 50 G, where the ratio of the magnetic moments of the two states is 2.5 and interactions are very weak. A magnetic field gradient is applied along the $z$-direction for about 4 ms, imparting a linear momentum of the same sign but a different magnitude to each spin state. The clouds are then allowed to evolve for about 30 ms, and they execute about half of an oscillation period at different amplitudes and frequencies (the frequency ratio is 1.6 between spin-up and spin-down). When the clouds have returned to the center of the trap, their centers of mass are displaced from each other by about 200 $\mu$m (for comparison, the $1/e$ radius of the majority cloud in the $z$-direction is between 200 and 300 $\mu$m at this point). A second gradient pulse is applied along the same direction to remove the relative velocity of the two clouds. The second pulse also removes most of the total center-of-mass motion. The total magnetic field is then ramped to the Feshbach resonance at 834 G in about 5 ms. At resonance, the two spin states have identical trapping frequencies of 22.8 Hz.[2]

To reach low temperatures, we apply a variable amount of evaporative cooling by lowering the depth of the optical dipole trap after reaching 834 G. The time available for evaporative cooling is limited to about 0.4 s by the relaxation time of the spin excitation. To reach high temperatures, we prepare a hotter cloud at 300 G and heat the system further at 834 G by releasing the atoms from the optical dipole trap and recapturing them. The depth of the optical dipole trap is then ramped gradually to a final value in 80 ms. The final depth is chosen to keep the number of atoms and the temperature approximately constant during the subsequent evolution, and it corresponds to an effective radial trap frequency ranging from 80 Hz for the low-temperature data to 250 Hz for the high-temperature data. After preparing the system at the chosen temperature and with a nonzero spin-dipole moment, we are left with typically $N_\uparrow \approx 4 \times 10^5$ atoms in the majority state and $N_\downarrow \approx 4 \times 10^4$ atoms in the minority state. We then allow the system to evolve for a variable wait time $t$ before measuring the densities of the spin-up and spin-down clouds using resonant absorption imaging. Note that we limit the

[2] The system as a whole oscillates harmonically along the $z$-direction at 22.8 Hz due to the residual center-of-mass energy. This motion does not affect the dynamics in the total center-of-mass frame because the trapping potential is harmonic in the $z$-direction, and therefore, according to Kohn's theorem, the dynamics in the total center-of-mass frame are equivalent to the dynamics of a system at rest [38].

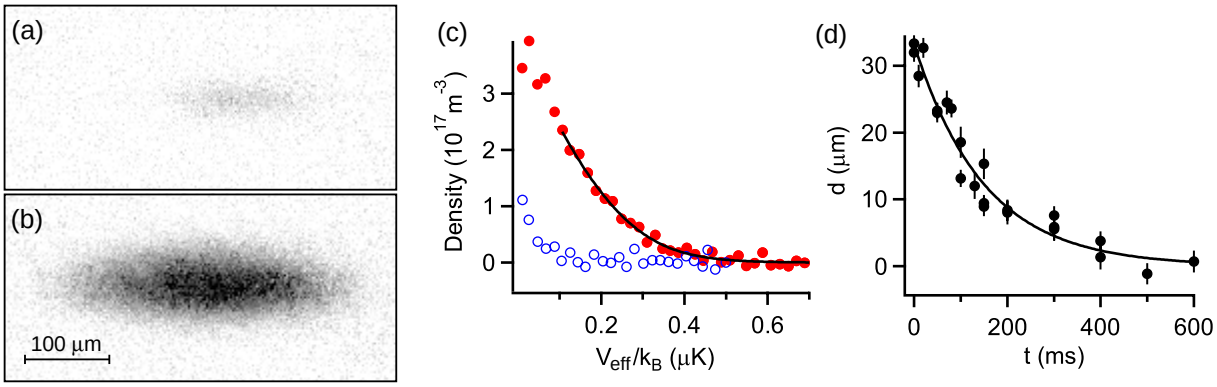


**Figure 1.** Measuring the spin-dipole mode of a highly polarized Fermi gas. (a) and (b) show 2D column density images of the minority and majority spin state, respectively, obtained using resonant absorption imaging in one run of the experiment. The imaging pulses are each 4 $\mu$s in duration and separated by 6 $\mu$s. The distance between the centers of mass in (a) and (b) is 34 $\mu$m. (c) Density of the majority (solid red circles) and minority (open blue circles) versus the effective potential energy $V_{\rm eff}$ defined in the text, obtained from the images in (a) and (b). The temperature of the cloud is found by fitting the non-interacting Fermi gas equation of state (solid line) to the region of the majority density where the minority fraction is 5% or less. (d) Displacement $d$ of the minority center of mass relative to the majority center of mass as a function of time $t$. This time series includes the run displayed in (a–c). Error bars are from fitting uncertainty (one std. dev.). The curve shows an exponential fit.

population of the majority cloud to ensure that the central optical density is less than 2, allowing for accurate density measurements.

Figures 1(a) and (b) show typical 2D column densities of the two spin states after evaporative cooling on resonance. From the column densities, we reconstruct the 3D densities $n_\sigma(\rho, z)$ of each state $\sigma = \uparrow, \downarrow$ using the inverse Abel transformation. The temperature of the system is determined by fitting the majority density as a function of potential energy to the equation of state of a non-interacting Fermi gas [37] (figure 1(c)): $n_{\uparrow,\rm FG} = -\lambda^{-3}\zeta_{3/2}(-e^{\beta(\mu - V_{\rm eff})})$, where $\lambda = \sqrt{2\pi\hbar^2/mk_BT}$ is the thermal de Broglie wavelength, $\beta = 1/k_BT$, the fit parameters are the chemical potential $\mu$ and the temperature $T$, $\zeta_{3/2}$ is the polylogarithm of order 3/2, and $V_{\rm eff} = V(\rho, z - Z_\uparrow)$ is the effective potential energy. The fit is restricted to $z < Z_\uparrow$ and to the outer edges of the majority cloud, where $n_\downarrow/n_\uparrow < x_c$. We used a cut-off minority fraction of $x_c = 0.05$ for all clouds with $T < 0.5T_{F\uparrow}$. For some of the data with $0.5 < T/T_{F\uparrow} < 1$, $x_c$ was increased to 0.08 to increase the available signal, while for the data with $T > 2T_{F\uparrow}$, $x_c$ was increased to 0.15 for the same reason. These increases in $x_c$ should not affect the accuracy of the thermometry because the system interacts less strongly at high $T/T_{F\uparrow}$ [3]. This is demonstrated by our spin susceptibility measurements for the balanced case in [14] that agree with the compressibility above $T/T_F \approx 1$, showing the absence of spin correlations in this temperature regime. For normalization, the central densities $n_\sigma(0)$ of each species are recorded and used to define the central Fermi energies $E_{F\sigma} = \hbar^2 k_{F\sigma}^2/2m_\sigma$, with $k_{F\sigma} = (6\pi^2 n_\sigma(0))^{1/3}$, $m_\uparrow = m$, and $m_\downarrow = m^*$, and Fermi temperatures $T_{F\sigma} = E_{F\sigma}/k_B$.

Spin transport is measured by observing the time evolution of the center-of-mass separation $d(t) = Z_\downarrow(t) - Z_\uparrow(t)$ (figure 1(d)), with $Z_{\uparrow(\downarrow)}(t)$ the center of mass of the majority (minority) cloud along the $z$-axis at time $t$, determined from a 2D Gaussian fit to the column density. We find that $d$ relaxes exponentially to zero, corresponding to an overdamped spin-dipole mode, and fit the evolution to an exponential function $d(t) = d_0 e^{-t/\tau}$. We report the dimensionless relaxation time $\tilde{\tau} = \hbar\omega_z^2\tau/E_{F\uparrow}$. Equation (3) implies that $\tilde{\tau}$ is mostly independent of the absolute scales set by the density and the trapping frequency. Defining the average momentum relaxation rate as

$$\frac{1}{\hat{\tau}_P} = \frac{\int d^3r\, n_\downarrow(\mathbf{r}) v_\downarrow(\mathbf{r})/\tau_P(\mathbf{r})}{\int d^3r\, n_\downarrow(\mathbf{r}) v_\downarrow(\mathbf{r})}, \tag{4}$$

and making the approximation that $\hat{\tau}_P$ is constant in time relates $\tilde{\tau}$ to fundamental properties of the system as

$$\tilde{\tau} \approx \frac{m^*/m}{(1+\alpha)} \cdot \frac{1/\hat{\tau}_P}{\hbar/E_{F\uparrow}}, \tag{5}$$

in the limit $(\omega_z\tau)^2 \gg 1$ realized in our measurements, where $\tau$ is always at least 100 ms, and so $(\omega_z\tau)^2 > 200$.

Figure 2 shows the measured values of the dimensionless relaxation time $\tilde{\tau}$ as a function of the reduced temperature $T/T_{F\uparrow}$. $\tilde{\tau}$ increases at low temperatures before reaching a maximum of $0.13(3)E_{F\uparrow}$ for $T/T_{F\uparrow} = 0.40(6)$, and decreases at higher temperatures. We interpret the behavior of the relaxation time at low temperatures as a consequence of Pauli blocking: as the temperature is lowered significantly below the majority Fermi temperature, the phase space available for a minority atom to scatter goes to zero. The reduction in $\tilde{\tau}$ at high temperatures is expected: at high temperatures, $1/\hat{\tau}_P$ is essentially given by the collision rate in the gas [40], $1/\hat{\tau}_P \sim n\sigma v$. The scattering cross-section $\sigma$ on resonance for $T \gg T_{F\uparrow}$ is given by the square of the de Broglie wavelength and is thus proportional to $1/T$, while the average speed $v$ of the particles is proportional to $\sqrt{T}$. Hence, $\tilde{\tau}$ is expected to decrease like $\hbar n\sigma v/E_{F\uparrow} \propto \sqrt{T_{F\uparrow}/T}$. We observed behavior similar to figure 2 in 3D Fermi gases with resonant interactions and equal spin populations in [14], although we see more significant Pauli blocking here than in [14] at comparable temperatures.

The systematic uncertainties of the measured values have been estimated, and are comparable to or less than the statistical errors. The temperature measurement uses knowledge of the potential energy (2). The radial potential energy function $V_\rho(\rho)$ is assumed to have the form

$$V_\rho(\rho) = \frac{2aP}{\pi w_0^2}(1 - e^{-2\rho^2/w_0^2}) - \frac{1}{4}m\omega_z^2\rho^2, \tag{6}$$

where $a$ is a known constant expressing the polarizability of the atoms, $P$ is the optical power of the dipole trap and $w_0$ is the waist of the trapping beam, and $\omega_z = 2\pi \times 22.8$ Hz is the axial trapping frequency. Direct measurements give $P$ and $w_0$ with 5–10% accuracy. To refine the trap model, we sum the 3D densities of the majority atom clouds for each value of $P$ used in the experiment, taking only $t > 190$ ms, and use the known axial potential together with the local density approximation to obtain $V_\rho(\rho)$. The model (6) is then fit to the experimentally measured $V_\rho(\rho)$ with $w_0$ as a free parameter, giving $w_0 = 115\,\mu$m. Equivalently, $P$ could have been used as the free parameter; the difference in the two approaches adds less than 1% uncertainty to the potential energy. The uncertainty in the potential energy is dominated by noise in the images of

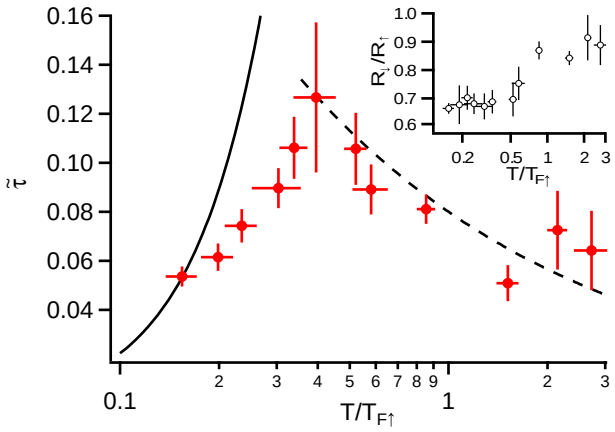


**Figure 2.** Normalized relaxation time of the spin-dipole mode of a highly polarized Fermi gas as a function of the reduced temperature $T/T_{\mathrm{F}\uparrow}$. $T_{\mathrm{F}\uparrow}$ is the local Fermi temperature at the center of the majority cloud. The solid curve is the low-temperature limit from [18], given by equation (7). The dashed curve is the expression $0.08\sqrt{\frac{T_{\mathrm{F}\uparrow}}{T}}$. The inset shows the average ratio of the minority cloud size to the majority cloud size as a function of the reduced temperature $T/T_{\mathrm{F}\uparrow}$. The cloud sizes are defined as the $1/e$ radii along the $z$-axis, estimated by fitting a 2D Gaussian function to the column densities of the two spin states. In both figures, each point is a weighted average of the results from 1 to 3 time series, with each time series containing on average 30 spin-up–spin-down image pairs. The error bars give standard deviations due to statistical fluctuations within a time series. Where the results of more than one time series are averaged, the error bars show the standard deviation of the weighted mean, determined from the standard deviations from each time series.

the clouds, giving an uncertainty in $w_0$ of about $2\,\mu$m. This implies a 7% systematic error on the potential energy at $\rho = 40\,\mu$m (a typical value of $\rho$ in the outer region of the cloud). The resulting systematic uncertainty on the temperature is 10% at the lowest temperatures, and 5% for temperatures near $T_{\mathrm{F}}$ or higher. Measurements of density are affected by the laser linewidth, imperfect polarization of the imaging light, and nonlinearities from saturation of the imaging transition, Doppler shifting of atoms scattered by the imaging light and pumping into transparent final states. The density measurement is calibrated using equilibrium low-temperature clouds with large spin imbalance. The systematic uncertainty in the density is 10%. This leads to a total systematic error in the reduced temperatures of 8–12%, and a systematic error in $\tilde{\tau}$ of 6%. The magnification of the imaging system is calibrated to 0.5% and does not contribute significantly to the uncertainties in $w_0$ or $d$.

It would be interesting to have available a calculation of spin transport coefficients such as $1/\tau_P$ at arbitrary temperatures for comparison with our data. A full solution is available for Fermi gases with equal populations in one spatial dimension [22, 23] and shows qualitative features similar to our data, with a maximum of the spin drag coefficient (analogous to $\tilde{\tau}$) at finite temperatures of the order of $T_{\mathrm{F}}$.

We expect our data to differ quantitatively from predictions for a homogeneous system. The measured quantity $\tilde{\tau}$ is a global property of the trapped system, while the momentum relaxation

rate $1/\tau_P$ is a local quantity. For $T \gg T_{F\uparrow}$, $1/\tau_P \propto n_\uparrow$, and $1/\tau_P$ increases with increasing majority density, while for $T \ll T_{F\uparrow}$, due to Pauli blocking $1/\tau_P \propto E_{F\uparrow}(T/T_{F\uparrow})^2 \propto n_\uparrow^{-2/3}$, and $1/\tau_P$ decreases with increasing majority density. Additionally, the variation in $1/\tau_P$ should cause the spin current to be non-uniform. The effect of inhomogeneity should be greater at high reduced temperatures, where the minority cloud size approaches the majority cloud size. The inset in figure 2 shows the ratio of the cloud sizes $R_\downarrow/R_\uparrow$ as a function of the reduced temperature, where $R_{\uparrow(\downarrow)}$ is the $1/e$ width in the $z$-direction from a 2D Gaussian fit to the majority (minority) column density. Indeed, $R_\downarrow/R_\uparrow$ increases with increasing $T/T_{F\uparrow}$. Even at the lowest temperatures, $R_\downarrow/R_\uparrow$ remains significant, attaining a value of 0.7, due to the finite minority fraction $N_\downarrow/N_\uparrow \approx 0.1$. The effect of inhomogeneity is therefore reduced at low temperatures, but should remain present.

We compare our results for $\tilde{\tau}$ at low temperatures to the low-temperature limit in [18], which can be written as

$$\frac{1/\tau_P(\mathbf{0})}{E_{F\uparrow}/\hbar} = c\frac{\alpha^2}{1+\alpha}\left(\frac{m^*}{m}\right)^2\left(\frac{T}{T_{F\uparrow}}\right)^2, \tag{7}$$

for temperatures $T \ll T_{F\uparrow}$.[3] The prefactor $c$ changes slightly from $c = \frac{2\pi^3}{9} = 6.89\ldots$ to c $\approx 6.0$ as the temperature rises from far below $T_{F\downarrow}$, where even the minority cloud is degenerate, to temperatures where $T_{F\downarrow} \ll T \ll T_{F\uparrow}$ and the minority is a classical gas [18]. In our coldest data, $T \approx 0.5T_{F\downarrow}$ and $T_{F\downarrow} \approx 0.3T_{F\uparrow}$, assuming $m^* = 1.2\,m$. To compare our data with [18], using (7), we set $c = \frac{2\pi^3}{9}$, $\alpha = 0.6$ and $m^* = 1.2\,m$. The comparison is affected by the inhomogeneous trapping potential in the experiment, as equation (7) gives the local value of $1/\tau_P$ at the center of the majority cloud. The experimental data agree with the value from equation (7) at the lowest temperatures measured (see figure 2). The deviation at higher temperatures is expected as the $T \ll T_{F\uparrow}$ limit becomes inapplicable. The convergence of the experimental data to the theoretical value at low temperature despite the inhomogeneity of the system may be partly due to the reduced minority cloud size at low temperatures, which reduces the effects of inhomogeneity, as discussed above. Additionally, the variation in the momentum relaxation rate with density will to some extent cancel at moderately low temperatures, as $1/\tau_P$ changes from increasing with increasing density at high reduced temperatures to decreasing with increasing density due to Pauli blocking at low reduced temperatures. The crossing of the experimental curve with the predictions for a uniform system at low temperatures therefore does not necessarily indicate that the inhomogeneity is negligible at low temperatures in this measurement.

At high temperatures $T \gg T_{F\uparrow,\downarrow}$, the spin transport properties of a trapped system can be calculated from the Boltzmann transport equation. For vanishing minority fraction, we find (now with $\alpha = 0$ and $m^* = m$ and assuming harmonic trapping in all three directions) [14]

$$\tilde{\tau} = \frac{8}{9\pi^{3/2}\epsilon}\sqrt{\frac{T_{F\uparrow}}{T}} \approx \frac{0.16}{\epsilon}\sqrt{\frac{T_{F\uparrow}}{T}}, \tag{8}$$

where $\epsilon = 1$ when the minority drift velocity distribution $v_\downarrow$ is uniform. This result features the expected dependence $\propto \sqrt{\frac{T_{F\uparrow}}{T}}$ on temperature. The relative velocity between the two spin states

[3] We omit a term due to the relative velocity of the spin up and spin-down clouds, which produces a correction of less than 1% in the overdamped, finite-temperature regime accessed in this experiment.

cannot be truly constant in space but has to be depressed in the center, where the density is highest and the momentum relaxation is fastest. In general,

$$\epsilon = \frac{\int \mathrm{d}^3 r\, v_\downarrow(\frac{\vec{r}}{\sqrt{2}})\mathrm{e}^{-\beta V}}{\int \mathrm{d}^3 r\, v_\downarrow(\vec{r})\mathrm{e}^{-\beta V}}, \tag{9}$$

where $V$ is the trapping potential (here assumed to be quadratic). For example, for a quadratic drift velocity profile, $v_\downarrow(\vec{r}) = ax^2 + by^2 + cz^2$, the predicted $\tilde{\tau}$ is reduced by factor of $\epsilon = 2$. We find that the high-temperature result (8) with $\epsilon = 2$ leads to close agreement with our experimental results (figure 2). This model is interesting because it estimates the effects of inhomogeneous density and velocity distributions, but it has shortcomings. The drift velocity should remain non-zero everywhere, rather than going to zero at the origin as in the quadratic case, and should have a radial component. A full quantitative description of the overdamped spin-dipole motion in the high-temperature limit in an external trapping potential will therefore be more complex.

### 3. A superfluid with small spin polarization

We extend the method of the previous section to study spin transport in Fermi gases with resonant interactions and small spin imbalance. When the global polarization $\frac{N_\uparrow - N_\downarrow}{N_\uparrow + N_\downarrow}$ is less than about 75% in a harmonically trapped Fermi gas at low temperature and with resonant interactions, the system phase separates into a superfluid core surrounded by a polarized normal state region [15, 16, 21]. The superfluid core is visible as a sharp reduction in the density difference of the two spin states [16]. The transition between the superfluid and the imbalanced normal regions forms a sharp interface below a tricritical point, where the density imbalance jumps between the two regions [39]. Scattering and spin transport at the interface between a normal and superfluid Fermi gas have been considered theoretically in [20, 41].

To observe spin transport in an imbalanced gas containing a superfluid, we prepare a spin mixture with a global polarization of 17(3)%. The gas is cooled at 300 G and again at 834 G after creating the spin-dipole excitation as described in the previous section. Two off-resonant phase contrast images are taken to measure the densities of each spin state. An imaging pulse tuned halfway between the resonance frequencies of the two states directly measures the difference in the column densities (figure 3(a)), while a second pulse, red-detuned from both states (figure 3(b)), provides additional information needed to reconstruct the total column density in each state [39]. From the column densities of each state, we obtain 3D density distributions using the inverse Abel transformation.

The 2D spin density (figure 3(a)) and 3D spin density (figure 3(c)) show a reduction near the center of the trap, with the 3D density going to zero, characteristic of the superfluid core in imbalanced Fermi gases [16]. We have checked that the shell structure remains even after the spin density reaches equilibrium. Additionally, we estimate the temperature $T$ of the system to confirm that it is cold enough to contain a superfluid. In unpolarized systems, the superfluid transition is predicted to occur at about $T_c/T_F = 0.173(6)$ [42], where $k_B T_F = E_F = \hbar^2(6\pi^2 n(0))^{2/3}/2m$ and $n$ is the density per spin state. This theoretical value agrees well with a determination of $T_c/T_F$ by our group. Fitting the equation of state of a unitary Fermi gas at zero imbalance [43] to the majority (minority) density gives an estimate $T_{\uparrow(\downarrow)}$ of the temperature. The fits are restricted to $V_{\sigma,\mathrm{eff}} > 0.3\,\mu$K, where $V_{\sigma,\mathrm{eff}} = V(\rho, z - Z_\sigma)$, to exclude

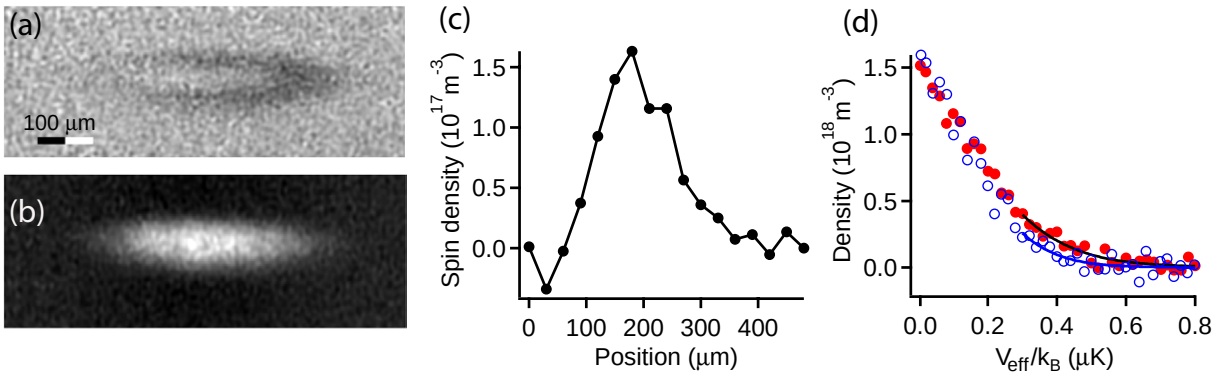


**Figure 3.** Spin-dipole mode of an imbalanced Fermi gas with a superfluid core. Phase contrast images are taken with imaging light detuned (a) halfway between the resonance frequencies of the two states and (b) at large red detuning from both states. The image in (a) is proportional to the difference in column densities of the two states. The depletion of the density difference in the center of the cloud indicates the superfluid region. It is displaced from the center of the majority due to the spin-dipole excitation. Panel (c) shows the difference in reconstructed 3D densities of the spin up and spin-down clouds as a function of the $z$ coordinate for $z > 0$. The depletion in the center again indicates pairing and superfluidity [16]. An elliptical average over a narrow range of the radial coordinate $\rho$ is used to increase the signal-to-noise ratio. (d) The temperature is estimated from the 3D densities of the two states as a function of the effective potential $V_{\mathrm{eff}}$ defined in the text. Solid red circles: majority density, open blue circles: minority density. The curves are fits to the densities using the equation of state of a unitary Fermi gas at zero imbalance to get upper and lower bounds on the temperature.

the putative superfluid region. Compared to a balanced gas at unitarity with $N'_\uparrow = N'_\downarrow = N_\uparrow$, and at the same temperature T, the majority cloud should have a larger size because the interaction energy between the spin-up and spin-down atoms is attractive. We therefore expect that $T_\uparrow$ is an overestimate of $T$. Likewise, we expect $T_\downarrow < T$, and we consider $T_\uparrow$ and $T_\downarrow$ to provide approximate upper and lower bounds on $T$.

Figure 4(a) shows the temperature bounds during the approach to equilibrium. Time-averaging gives $0.12(1) < T/T_{\mathrm{F}} < 0.15(2)$, where $T_{\mathrm{F}} \equiv T_{\mathrm{F}\uparrow} \approx T_{\mathrm{F}\downarrow}$. The error estimates include the standard error of the mean and the systematic error from uncertainty in the potential energy and in the density. These temperature bounds confirm that the system is in the vicinity of the superfluid transition.

Even in the presence of the superfluid core, we still observe strong damping of the spin-dipole mode. Figure 4(b) shows that the displacement $d$ between the majority and minority centers of mass along the $z$-axis relaxes gradually to zero, rather than oscillating as would be expected in a dissipationless system. The $1/e$ relaxation time $\tau = 360\,\mathrm{ms}$ corresponds to a spin drag coefficient [13, 22] of $\omega_z^2\tau = 0.06(1)E_{\mathrm{F}\uparrow}/\hbar$, close to the maximum spin drag coefficient in non-polarized trapped Fermi gases at unitarity [14].

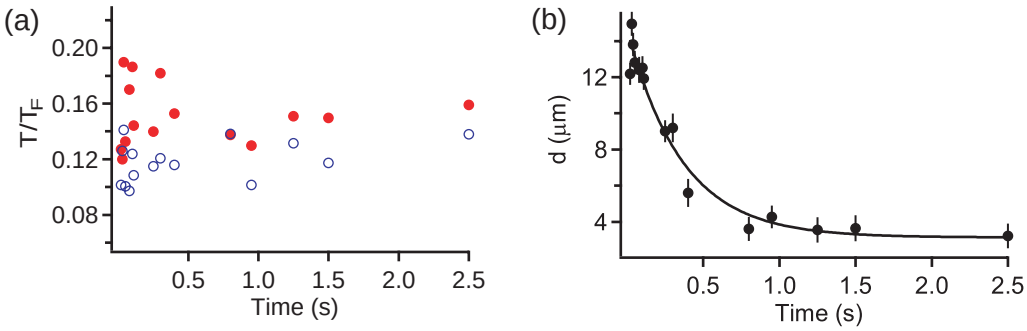


**Figure 4.** (a) Reduced temperature as a function of time during relaxation of the spin-dipole excitation in a spin-polarized Fermi gas containing a superfluid region. Red solid (blue open) circles: $T_{\uparrow(\downarrow)}/T_{F\uparrow(\downarrow)}$ from a fit to the edge of the majority (minority) spin state using the equation of state of an unpolarized unitary Fermi gas, giving an upper (lower) limit to true temperature. (b) The displacement of the spin-up and spin-down centers of mass relaxes exponentially, indicating strong spin drag despite the presence of a superfluid. Error bars: one std. dev. from fitting error.

The strong damping is reminiscent of the friction between the normal and superfluid component in liquid helium [44] and in atomic Bose–Einstein condensates [46]. In the latter case, out-of-phase oscillations between the condensate and the thermal component are strongly damped. Even at low temperatures, currents in superfluids as well as in 1D superconducting wires are still damped due to phase slips [46–48]. In the presented case of a partially polarized Fermi gas, Andreev reflection of unpaired atoms at the normal-to-superfluid interface should cause spin current decay even at the lowest temperatures [20, 41]. At higher temperatures or if the majority chemical potential in the normal state region can overcome the pairing gap, the microscopic velocity of majority atoms will significantly exceed the critical velocity of the superfluid of about $0.3v_F$ [49, 50], causing strong dissipation of spin currents. The relative importance of dissipation at the interface versus dissipation inside the superfluid could be determined by whether a spin current flows through the superfluid or around it. However, we are not able to determine the spatial distribution of the spin current with our current data.

## 4. Conclusions

In this work, we presented our measurements on the damping of the spin-dipole mode in a highly polarized Fermi gas with resonant interactions, over a wide range of temperatures. The damping is seen to become weaker at temperatures significantly less than the majority Fermi energy, as expected from Pauli blocking, i.e. the fact that quasi-particles in a Fermi liquid become long lived at sufficiently low temperatures. These measurements provide the first quantitative test of theoretical calculations of the spin transport properties of highly polarized Fermi gases. We also observe spin transport in a Fermi gas with low spin polarization containing a superfluid region. It is found that the spin-dipole motion remains strongly damped, revealing the importance of friction between the superfluid and the normal component, possibly accompanied by reflection processes at the interface.

## Acknowledgments

This work was supported by the NSF, AFOSR-MURI, AFOSR-YIP, ARO-MURI, ONR, DARPA YFA, a grant from the Army Research Office with funding from the DARPA OLE program, the David and Lucille Packard Foundation and the Alfred P Sloan Foundation. The authors thank André Schirotzek, Giacomo Roati and Peyman Ahmadi for experimental assistance and David Huse for interesting discussions.

## References

[1] Chin C, Grimm R, Julienne P and Tiesinga E 2010 Feshbach resonances in ultracold gases *Rev. Mod. Phys.* **82** 1225–86
[2] Ketterle W and Zwierlein M W 2008 Making, probing and understanding ultracold Fermi gases *Ultracold Fermi Gases, Proc. Int. School of Physics 'Enrico Fermi', Course CLXIV (Varenna, 20–30 June 2006)* ed M Inguscio, W Ketterle and C Salomon (Amsterdam: IOS Press) pp 1–462
[3] Giorgini S, Pitaevskii L P and Stringari S 2008 Theory of ultracold atomic Fermi gases *Rev. Mod. Phys.* **80** 1215–60
[4] Cao C, Elliott E, Joseph J, Wu H, Petricka J, Schäfer T and Thomas J E 2010 Universal quantum viscosity in a unitary Fermi gas *Science* **331** 58–61
[5] O'Hara K M, Hemmer S L, Gehm M E, Granade S R and Thomas J E 2002 Observation of a strongly interacting degenerate Fermi gas of atoms *Science* **298** 2179
[6] Kinast J, Hemmer S L, Gehm M E, Turlapov A and Thomas J E 2004 Evidence for superfluidity in a resonantly interacting Fermi gas *Phys. Rev. Lett.* **92** 150402
[7] Bartenstein M, Altmeyer A, Riedl S, Jochim S, Chin C, Hecker-Denschlag J and Grimm R 2004 Collective excitations of a degenerate gas at the BEC-BCS crossover *Phys. Rev. Lett.* **92** 203201
[8] Altmeyer A, Riedl S, Kohstall C, Wright M J, Geursen R, Bartenstein M, Chin C, Hecker J Denschlag and Grimm R 2007 Precision measurements of collective oscillations in the BEC-BCS crossover *Phys. Rev. Lett.* **98** 040401
[9] Zwierlein M W, Abo-Shaeer J R, Schirotzek A, Schunck C H and Ketterle W 2005 Vortices and superfluidity in a strongly interacting Fermi gas *Nature* **435** 1047–51
[10] DeMarco B and Jin D S 2002 Spin excitations in a Fermi gas of atoms *Phys. Rev. Lett.* **88** 040405
[11] Gensemer S D and Jin D S 2001 Transition from collisionless to hydrodynamic behavior in an ultracold Fermi gas *Phys. Rev. Lett.* **87** 173201
[12] Du X, Luo L, Clancy B and Thomas J E 2008 Observation of anomalous spin segregation in a trapped Fermi gas *Phys. Rev. Lett.* **101** 150401
[13] D'Amico I and Vignale G 2000 Theory of spin Coulomb drag in spin-polarized transport *Phys. Rev.* B **62** 4853–7
[14] Sommer A, Ku M, Roati G and Zwierlein M W 2011 Universal spin transport in a strongly interacting Fermi gas *Nature* **472** 201–4
[15] Zwierlein M W, Schirotzek A, Schunck C H and Ketterle W 2006 Fermionic superfluidity with imbalanced spin populations *Science* **311** 492–6
[16] Shin Y, Zwierlein M W, Schunck C H, Schirotzek A and Ketterle W 2006 Observation of phase separation in a strongly interacting imbalanced Fermi gas *Phys. Rev. Lett.* **97** 030401
[17] Schirotzek A, Wu C-H, Sommer A and Zwierlein M W 2009 Observation of Fermi polarons in a tunable Fermi liquid of ultracold atoms *Phys. Rev. Lett.* **102** 230402–4
[18] Bruun G M, Recati A, Petchick C J, Smith H and Stringari S 2008 Collisional properties of a polarized Fermi gas with resonant interactions *Phys. Rev. Lett.* **100** 240406
[19] Recati A, Lobo C and Stringari S 2008 Role of interactions in spin-polarized atomic Fermi gases at unitarity *Phys. Rev.* A **78** 023633

[20] Parish M M and Huse D A 2009 Evaporative depolarization and spin transport in a unitary trapped Fermi gas *Phys. Rev.* A **80** 063605
[21] Nascimbène S, Navon N, Jiang K J, Tarruell L, Teichmann M, McKeever J, Chevy F and Salomon C 2009 Collective oscillations of an imbalanced Fermi gas: axial compression modes and polaron effective mass *Phys. Rev. Lett.* **103** 170402–4
[22] Polini M and Vignale G 2007 Spin drag and spin-charge separation in cold Fermi gases *Phys. Rev. Lett.* **98** 266403
[23] Rainis D, Polini M, Tosi M P and Vignale G 2008 Spin-drag relaxation time in one-dimensional spin-polarized Fermi gases *Phys. Rev.* B **77** 035113
[24] Duine R A, Polini M, Stoof H T C and Vignale G 2010 Spin drag in an ultracold Fermi gas on the verge of ferromagnetic instability *Phys. Rev. Lett.* **104** 220403
[25] Clogston A M 1962 Upper limit for the critical field in hard superconductors *Phys. Rev. Lett.* **9** 266
[26] Chandrasekhar B S 1962 A note on the maximum critical field of high-field superconductors *Appl. Phys. Lett.* **1** 7
[27] Chevy F 2006 Universal phase diagram of a strongly interacting Fermi gas with unbalanced spin populations *Phys. Rev.* A **74** 063628
[28] Combescot R, Recati A, Lobo C and Chevy F 2007 Normal state of highly polarized Fermi gases: simple many-body approaches *Phys. Rev. Lett.* **98** 180402
[29] Prokof'ev N and Svistunov B 2008 Fermi-polaron problem: diagrammatic Monte Carlo method for divergent sign-alternating series *Phys. Rev.* B **77** 020408
[30] Lobo C, Recati A, Giorgini S and Stringari S 2006 Normal state of a polarized Fermi gas at unitarity *Phys. Rev. Lett.* **97** 200403
[31] Shin Y-I 2008 Determination of the equation of state of a polarized Fermi gas at unitarity *Phys. Rev.* A **77** 041603
[32] Nascimbène S, Navon N, Jiang K J, Chevy F and Salomon C 2010 Exploring the thermodynamics of a universal Fermi gas *Nature* **463** 1057–60
[33] Combescot R and Giraud S 2008 Normal state of highly polarized Fermi gases: full many-body treatment *Phys. Rev. Lett.* **101** 050404
[34] Prokof'ev N V and Svistunov B V 2008 Bold diagrammatic Monte Carlo: a generic sign-problem tolerant technique for polaron models and possibly interacting many-body problems *Phys. Rev.* B **77** 125101
[35] Pilati S and Giorgini S 2008 Phase separation in a polarized Fermi gas at zero temperature *Phys. Rev. Lett.* **100** 030401
[36] Hadzibabic Z, Gupta S, Stan C A, Schunck C H, Zwierlein M W, Dieckmann K and Ketterle W 2003 Fifty-fold improvement in the number of quantum degenerate fermionic atoms *Phys. Rev. Lett.* **91** 160401
[37] Zwierlein M W, Schunck C H, Schirotzek A and Ketterle W 2006 Direct observation of the superfluid phase transition in ultracold Fermi gases *Nature* **442** 54–8
[38] Dobson J F 1994 Harmonic-potential theorem: implications for approximate many-body theories *Phys. Rev. Lett.* **73** 2244
[39] Shin Y-I, Schunck C H, Schirotzek A and Ketterle W 2008 Phase diagram of a two-component Fermi gas with resonant interactions *Nature* **451** 689–93
[40] Vichi L and Stringari S 1999 Collective oscillations of an interacting trapped Fermi gas *Phys. Rev.* A **60** 4734
[41] Van Schaeybroeck B and Lazarides A 2007 Normal-superfluid interface scattering for polarized fermion gases *Phys. Rev. Lett.* **98** 170402
[42] Goulko O and Wingate M 2010 Thermodynamics of balanced and slightly spin-imbalanced Fermi gases at unitarity *Phys. Rev.* A **82** 053621
[43] Ku M, Schirotzek A, Sommer A, Zwierlein M, Van K Houcke, Werner F, Kozik E, Prokofev N and Svistunov B 2010 equation of state of a strongly interacting atomic Fermi gas, available at http://meetings.aps.org/link/BAPS.2010.DAMOP.W6.1
[44] Vinen W F 1957 Mutual friction in a heat current in liquid helium ii. iii theory of mutual friction *Proc. R. Soc.* A **242** 493–515

[45] Stamper-Kurn D M, Miesner H-J, Inouye S, Andrews M R and Ketterle W 1998 Collisionless and hydrodynamic excitations of a Bose–Einstein condensate *Phys. Rev. Lett.* **81** 500–3
[46] Langer J S and Michael Fisher E 1967 Intrinsic critical velocity of a superfluid *Phys. Rev. Lett.* **19** 560–3
[47] Langer J S and Ambegaokar V 1967 Intrinsic resistive transition in narrow superconducting channels *Phys. Rev.* **164** 498–510
[48] McKay D, White M, Pasienski M and DeMarco B 2008 Phase-slip-induced dissipation in an atomic Bose–Hubbard system *Nature* **453** 76–80
[49] Miller D E, Chin J K, Stan C A, Liu Y, Setiawan W, Sanner C and Ketterle W 2007 Critical velocity for superfluid flow across the BEC-BCS crossover *Phys. Rev. Lett.* **99** 070402
[50] Combescot R, Kagan M Yu and Stringari S 2006 Collective mode of homogeneous superfluid Fermi gases in the BEC-BCS crossover *Phys. Rev.* A **74** 042717

Spin transport in polaronic and superfluid Fermi gases



2011 New J. Phys. 13 055009

(http://iopscience.iop.org/1367-2630/13/5/055009)

New Journal of Physics
The open-access journal for physics

# Spin transport in polaronic and superfluid Fermi gases

**Ariel Sommer**[1], **Mark Ku and Martin W Zwierlein**
Department of Physics, MIT-Harvard Center for Ultracold Atoms, MIT, Cambridge, MA 02139, USA
and
Research Laboratory of Electronics, MIT, Cambridge, MA 02139, USA
E-mail: atsommer@mit.edu

*New Journal of Physics* **13** (2011) 055009 (14pp)
Received 10 February 2011
Published 24 May 2011
Online at http://www.njp.org/
doi:10.1088/1367-2630/13/5/055009

**Abstract.** We present measurements of spin transport in ultracold gases of fermionic $^6$Li in a mixture of two spin states at a Feshbach resonance. In particular, we study the spin-dipole mode, where the two spin components are displaced from each other against a harmonic restoring force. We prepare a highly imbalanced, or polaronic, spin mixture with a spin-dipole excitation and we observe strong, unitarity-limited damping of the spin-dipole mode. In gases with small spin imbalance, below the Pauli limit for superfluidity, we observe strongly damped spin flow even in the presence of a superfluid core. This indicates strong mutual friction between superfluid and polarized normal spins, possibly involving Andreev reflection at the superfluid–normal interface.

**Contents**



[1] Author to whom any correspondence should be addressed.

## 1. Introduction

The quality of transport is one of the most important properties distinguishing states of matter. Of great technical importance, electrons in condensed matter materials can flow as currents or supercurrents, or be localized in an insulator, or even switch their state of conductivity through controllable parameters like an applied magnetic field. It is the task of many-body physics to develop models that may explain the observed transport properties in a system. Dilute atomic gases cooled to quantum degeneracy provide ideal systems for testing many-body theories. In particular, Feshbach resonances [1] in atomic Fermi gases allow experimental control over the strength of two-body interactions, giving access to the Bose–Einstein condensation to Bardeen–Cooper–Schrieffer superfluid (BEC–BCS) crossover regime [2, 3]. Transport properties have played an important role in characterizing strongly interacting Fermi gases in the BEC-BCS crossover, with the observation of hydrodynamic flow indicating nearly perfect fluidity [4, 5], the measurement of collective excitation frequencies probing the equation of state [6–8], and the observation of vortex lattices in rotating gases demonstrating superfluidity [9]. The first observations of spin transport in Fermi gases were obtained in the weakly interacting regime, and showed the onset of Pauli blocking of collisions [10], and the transition from collisionless to hydrodynamic behavior [11]. Spin excitations have also been observed in Fermi gases as long-lived spin waves near zero scattering length [12].

Here we study spin transport in strongly interacting two-component Fermi gases. Spin currents are strongly damped in such systems due to the high collision rate between opposite spin atoms: as two-body scattering does not conserve relative momentum, each scattering event on average reduces the net spin current [13]. At the Feshbach resonance, scattering is maximal, with a mean-free path between collisions of opposite spins that can be as short as one interparticle spacing—the smallest possible in a three-dimensional (3D) gas. Measurements of spin transport in strongly interacting Fermi gases with an equal number of atoms in two spin states were recently reported [14]. Interactions were shown to be strong enough to reverse spin currents, with two clouds of opposite spin almost perfectly repelling each other. The spin diffusivity was found to reach a lower limit of the order of $\hbar/m$ at unitarity, the quantum limit of diffusion. Here, we consider the case where the number of atoms in the two states is unequal, and study spin transport in the polaron and phase-separated superfluid regimes. In highly polarized systems that remain non-superfluid down to zero temperature [15–17], spin currents are expected to become undamped due to Pauli blocking [18–20]. In this imbalanced regime, a high-frequency mode observed after a compressional excitation was interpreted as a weakly damped spin quadrupole (or breathing) mode [21]. The question of the damping properties of the spin excitation and its temperature dependence was left open. Spin transport properties of ultracold Fermi gases have been investigated theoretically most recently in [18–20], [22–24], allowing comparison between theory and experiment.

In section 2, we present measurements of the damping rate of spin excitations in highly polarized Fermi gases as a function of temperature. We show that damping is maximal at finite temperatures. In section 3, we study smaller spin polarizations, below the Pauli limit of superfluidity [15], just enough to reveal the presence of a superfluid core in the system. We show that the spin-dipole mode is strongly damped in the presence of the superfluid. In a partially polarized Fermi gas, damping of spin motion is expected to persist at low temperatures due to Andreev reflection [20].

## 2. Highly imbalanced Fermi gases

Fermi gases with resonant interactions can remain normal down to zero temperature if the spin imbalance exceeds the Pauli (or the Clogston–Chandrasekhar) limit [15, 16, 21, 25, 26, 39]. We refer to the spin state with the larger population of atoms as the majority, or spin-up state, and the state with fewer atoms as the minority, or spin-down state. Radio-frequency (RF) spectroscopy [17] on such systems confirms the quasi-particle picture [27–29] where minority atoms are dressed by the majority Fermi sea, forming a quasi-particle known as the Fermi polaron. The energy of a single polaron in a zero-temperature Fermi sea of spin-up atoms has been described using the effective Hamiltonian [18, 19, 30],

$$H = -\alpha\mu_\uparrow + \frac{\mathbf{p}^2}{2m^*}, \tag{1}$$

where $\mathbf{p}$ is the momentum of the polaron, $m^*$ is the polaron effective mass, $\mu_\uparrow$ is the local spin-up chemical potential and $\alpha$ characterizes the polaron binding energy. The parameters $\alpha$ and $m^*/m$, where $m$ is the bare mass of spin-up and spin-down fermions, have been measured experimentally [17, 21, 31, 32] and calculated theoretically [30], [33–35], giving $\alpha = 0.62$ and $m^*/m \approx 1.2$ at zero temperature.

We consider a mixture of $N_\uparrow$ spin-up fermions and $N_\downarrow$ spin-down fermions at temperature $T$ with equal masses and resonant interactions, held in a spin-independent potential of the form

$$V(\rho, z) = \tfrac{1}{2}m\omega_z^2 z^2 + V_\rho(\rho), \tag{2}$$

where $\rho^2 = x^2 + y^2$. The spin-up (down) clouds have density $n_{\uparrow(\downarrow)}(\mathbf{r})$ at position $\mathbf{r}$. The minority cloud is initially displaced by a small amount $Z_\downarrow(0)$ along the $z$-axis and is allowed to relax to its equilibrium position.

In the limit $N_\downarrow \ll N_\uparrow$, the motion of the spin-up cloud due to momentum absorbed from the spin-down cloud may be neglected. The equation of motion of the spin-down center of mass $Z_\downarrow$ is then [18]

$$m^*\ddot{Z}_\downarrow + (1+\alpha)m\omega_z^2 Z_\downarrow + \frac{m^*}{N_\downarrow}\int \mathrm{d}^3 r\, n_\downarrow(\mathbf{r})\frac{v_\downarrow(\mathbf{r})}{\tau_P(\mathbf{r})} = 0, \tag{3}$$

where the factor of $(1+\alpha)$ is due to the attraction of the minority fermions to the majority cloud, $1/\tau_P$ is the local momentum relaxation rate due to collisions [18] and is equivalent to the spin drag coefficient [13, 22], and $v_\downarrow$ is the local drift velocity of spin-down atoms. By dimensional analysis, $\hbar/\tau_P(\mathbf{r})$ must be given by the local majority Fermi energy times a universal dimensionless function of the local reduced temperature $T/T_{\mathrm{F}\uparrow}^{\mathrm{local}}(\mathbf{r})$ and the local ratio $T_{\mathrm{F}\downarrow}^{\mathrm{local}}(\mathbf{r})/T_{\mathrm{F}\uparrow}^{\mathrm{local}}(\mathbf{r})$ of the Fermi temperatures, where $T_{\mathrm{F}\uparrow(\downarrow)}^{\mathrm{local}}(\mathbf{r})$ is the local majority (minority) Fermi temperature. The first two terms in (3) follow from (1), (2) and the local density approximation, while the third term is due to damping and is not captured in (1). Equation (3) neglects a possible back-action of the minority on the majority atoms that might deform the majority density profile.

In our experimental realization of this transport problem, we use a gas of ultracold fermionic $^6$Li atoms. The $^6$Li atoms are cooled sympathetically with $^{23}$Na [36] and loaded into a hybrid optical and magnetic trap with an adjustable bias magnetic field [37]. The magnetic field curvature provides essentially perfect harmonic confinement along the axial ($z$) direction, while the optical dipole trap (laser wavelength 1064 nm, waist 115 $\mu$m) provides trapping in the radial

directions, with negligible contribution to the axial confinement. With this system, we perform a collection of time series measurements. In each time series, we prepare the system in a chosen initial state and observe its evolution.

At the Feshbach resonance at 834 G, the magnetic moments of 'spin-up' and 'spin-down' atoms, the two lowest hyperfine states of $^6$Li, are equal to 1 part in 1000, since their electron spin is in fact aligned with the magnetic field. Inducing a spin current is therefore extremely challenging on resonance. However, at lower fields, their magnetic moments differ, allowing separation of the two gas clouds by a magnetic field gradient. Our experimental procedure for producing these separated clouds is as follows.

We prepare the system starting with about $1 \times 10^7$ atoms of $^6$Li in the lowest hyperfine state, at a total magnetic field of 300 G. A small fraction of atoms are transferred to the second-lowest hyperfine state using a RF Landau–Zener sweep. The mixture is then evaporatively cooled for a variable amount of time by lowering the depth of the optical dipole trap from $k_B \times 7\,\mu$K to a variable final depth between $k_B \times 0.5\,\mu$K and $k_B \times 1\,\mu$K, where $k_B$ is the Boltzmann constant. The optical dipole trap depth is then raised to $k_B \times 6\,\mu$K, where the zero-temperature Fermi energy in the majority state is between $k_B \times 0.8\,\mu$K and $k_B \times 1.3\,\mu$K.

After the spin mixture is prepared at 300 G, the total magnetic field is reduced gradually over 500 ms to 50 G, where the ratio of the magnetic moments of the two states is 2.5 and interactions are very weak. A magnetic field gradient is applied along the $z$-direction for about 4 ms, imparting a linear momentum of the same sign but a different magnitude to each spin state. The clouds are then allowed to evolve for about 30 ms, and they execute about half of an oscillation period at different amplitudes and frequencies (the frequency ratio is 1.6 between spin-up and spin-down). When the clouds have returned to the center of the trap, their centers of mass are displaced from each other by about 200 $\mu$m (for comparison, the $1/e$ radius of the majority cloud in the $z$-direction is between 200 and 300 $\mu$m at this point). A second gradient pulse is applied along the same direction to remove the relative velocity of the two clouds. The second pulse also removes most of the total center-of-mass motion. The total magnetic field is then ramped to the Feshbach resonance at 834 G in about 5 ms. At resonance, the two spin states have identical trapping frequencies of 22.8 Hz.[2]

To reach low temperatures, we apply a variable amount of evaporative cooling by lowering the depth of the optical dipole trap after reaching 834 G. The time available for evaporative cooling is limited to about 0.4 s by the relaxation time of the spin excitation. To reach high temperatures, we prepare a hotter cloud at 300 G and heat the system further at 834 G by releasing the atoms from the optical dipole trap and recapturing them. The depth of the optical dipole trap is then ramped gradually to a final value in 80 ms. The final depth is chosen to keep the number of atoms and the temperature approximately constant during the subsequent evolution, and it corresponds to an effective radial trap frequency ranging from 80 Hz for the low-temperature data to 250 Hz for the high-temperature data. After preparing the system at the chosen temperature and with a nonzero spin-dipole moment, we are left with typically $N_\uparrow \approx 4 \times 10^5$ atoms in the majority state and $N_\downarrow \approx 4 \times 10^4$ atoms in the minority state. We then allow the system to evolve for a variable wait time $t$ before measuring the densities of the spin-up and spin-down clouds using resonant absorption imaging. Note that we limit the

[2] The system as a whole oscillates harmonically along the $z$-direction at 22.8 Hz due to the residual center-of-mass energy. This motion does not affect the dynamics in the total center-of-mass frame because the trapping potential is harmonic in the $z$-direction, and therefore, according to Kohn's theorem, the dynamics in the total center-of-mass frame are equivalent to the dynamics of a system at rest [38].

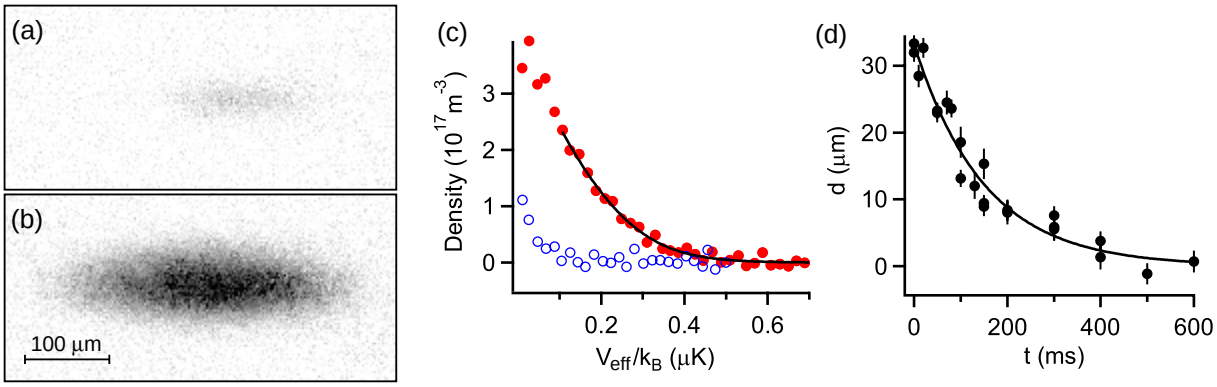


**Figure 1.** Measuring the spin-dipole mode of a highly polarized Fermi gas. (a) and (b) show 2D column density images of the minority and majority spin state, respectively, obtained using resonant absorption imaging in one run of the experiment. The imaging pulses are each 4 $\mu$s in duration and separated by 6 $\mu$s. The distance between the centers of mass in (a) and (b) is 34 $\mu$m. (c) Density of the majority (solid red circles) and minority (open blue circles) versus the effective potential energy $V_{\rm eff}$ defined in the text, obtained from the images in (a) and (b). The temperature of the cloud is found by fitting the non-interacting Fermi gas equation of state (solid line) to the region of the majority density where the minority fraction is 5% or less. (d) Displacement $d$ of the minority center of mass relative to the majority center of mass as a function of time $t$. This time series includes the run displayed in (a–c). Error bars are from fitting uncertainty (one std. dev.). The curve shows an exponential fit.

population of the majority cloud to ensure that the central optical density is less than 2, allowing for accurate density measurements.

Figures 1(a) and (b) show typical 2D column densities of the two spin states after evaporative cooling on resonance. From the column densities, we reconstruct the 3D densities $n_\sigma(\rho, z)$ of each state $\sigma = \uparrow, \downarrow$ using the inverse Abel transformation. The temperature of the system is determined by fitting the majority density as a function of potential energy to the equation of state of a non-interacting Fermi gas [37] (figure 1(c)): $n_{\uparrow,\rm FG} = -\lambda^{-3}\zeta_{3/2}(-e^{\beta(\mu - V_{\rm eff})})$, where $\lambda = \sqrt{2\pi\hbar^2/mk_BT}$ is the thermal de Broglie wavelength, $\beta = 1/k_BT$, the fit parameters are the chemical potential $\mu$ and the temperature $T$, $\zeta_{3/2}$ is the polylogarithm of order 3/2, and $V_{\rm eff} = V(\rho, z - Z_\uparrow)$ is the effective potential energy. The fit is restricted to $z < Z_\uparrow$ and to the outer edges of the majority cloud, where $n_\downarrow/n_\uparrow < x_c$. We used a cut-off minority fraction of $x_c = 0.05$ for all clouds with $T < 0.5T_{F\uparrow}$. For some of the data with $0.5 < T/T_{F\uparrow} < 1$, $x_c$ was increased to 0.08 to increase the available signal, while for the data with $T > 2T_{F\uparrow}$, $x_c$ was increased to 0.15 for the same reason. These increases in $x_c$ should not affect the accuracy of the thermometry because the system interacts less strongly at high $T/T_{F\uparrow}$ [3]. This is demonstrated by our spin susceptibility measurements for the balanced case in [14] that agree with the compressibility above $T/T_F \approx 1$, showing the absence of spin correlations in this temperature regime. For normalization, the central densities $n_\sigma(0)$ of each species are recorded and used to define the central Fermi energies $E_{F\sigma} = \hbar^2 k_{F\sigma}^2/2m_\sigma$, with $k_{F\sigma} = (6\pi^2 n_\sigma(0))^{1/3}$, $m_\uparrow = m$, and $m_\downarrow = m^*$, and Fermi temperatures $T_{F\sigma} = E_{F\sigma}/k_B$.

Spin transport is measured by observing the time evolution of the center-of-mass separation $d(t) = Z_\downarrow(t) - Z_\uparrow(t)$ (figure 1(d)), with $Z_{\uparrow(\downarrow)}(t)$ the center of mass of the majority (minority) cloud along the $z$-axis at time $t$, determined from a 2D Gaussian fit to the column density. We find that $d$ relaxes exponentially to zero, corresponding to an overdamped spin-dipole mode, and fit the evolution to an exponential function $d(t) = d_0 e^{-t/\tau}$. We report the dimensionless relaxation time $\tilde{\tau} = \hbar\omega_z^2\tau/E_{F\uparrow}$. Equation (3) implies that $\tilde{\tau}$ is mostly independent of the absolute scales set by the density and the trapping frequency. Defining the average momentum relaxation rate as

$$\frac{1}{\hat{\tau}_P} = \frac{\int d^3r\, n_\downarrow(\mathbf{r}) v_\downarrow(\mathbf{r})/\tau_P(\mathbf{r})}{\int d^3r\, n_\downarrow(\mathbf{r}) v_\downarrow(\mathbf{r})}, \tag{4}$$

and making the approximation that $\hat{\tau}_P$ is constant in time relates $\tilde{\tau}$ to fundamental properties of the system as

$$\tilde{\tau} \approx \frac{m^*/m}{(1+\alpha)} \cdot \frac{1/\hat{\tau}_P}{\hbar/E_{F\uparrow}}, \tag{5}$$

in the limit $(\omega_z\tau)^2 \gg 1$ realized in our measurements, where $\tau$ is always at least 100 ms, and so $(\omega_z\tau)^2 > 200$.

Figure 2 shows the measured values of the dimensionless relaxation time $\tilde{\tau}$ as a function of the reduced temperature $T/T_{F\uparrow}$. $\tilde{\tau}$ increases at low temperatures before reaching a maximum of $0.13(3)E_{F\uparrow}$ for $T/T_{F\uparrow} = 0.40(6)$, and decreases at higher temperatures. We interpret the behavior of the relaxation time at low temperatures as a consequence of Pauli blocking: as the temperature is lowered significantly below the majority Fermi temperature, the phase space available for a minority atom to scatter goes to zero. The reduction in $\tilde{\tau}$ at high temperatures is expected: at high temperatures, $1/\hat{\tau}_P$ is essentially given by the collision rate in the gas [40], $1/\hat{\tau}_P \sim n\sigma v$. The scattering cross-section $\sigma$ on resonance for $T \gg T_{F\uparrow}$ is given by the square of the de Broglie wavelength and is thus proportional to $1/T$, while the average speed $v$ of the particles is proportional to $\sqrt{T}$. Hence, $\tilde{\tau}$ is expected to decrease like $\hbar n\sigma v/E_{F\uparrow} \propto \sqrt{T_{F\uparrow}/T}$. We observed behavior similar to figure 2 in 3D Fermi gases with resonant interactions and equal spin populations in [14], although we see more significant Pauli blocking here than in [14] at comparable temperatures.

The systematic uncertainties of the measured values have been estimated, and are comparable to or less than the statistical errors. The temperature measurement uses knowledge of the potential energy (2). The radial potential energy function $V_\rho(\rho)$ is assumed to have the form

$$V_\rho(\rho) = \frac{2aP}{\pi w_0^2}(1 - e^{-2\rho^2/w_0^2}) - \frac{1}{4}m\omega_z^2\rho^2, \tag{6}$$

where $a$ is a known constant expressing the polarizability of the atoms, $P$ is the optical power of the dipole trap and $w_0$ is the waist of the trapping beam, and $\omega_z = 2\pi \times 22.8$ Hz is the axial trapping frequency. Direct measurements give $P$ and $w_0$ with 5–10% accuracy. To refine the trap model, we sum the 3D densities of the majority atom clouds for each value of $P$ used in the experiment, taking only $t > 190$ ms, and use the known axial potential together with the local density approximation to obtain $V_\rho(\rho)$. The model (6) is then fit to the experimentally measured $V_\rho(\rho)$ with $w_0$ as a free parameter, giving $w_0 = 115\,\mu$m. Equivalently, $P$ could have been used as the free parameter; the difference in the two approaches adds less than 1% uncertainty to the potential energy. The uncertainty in the potential energy is dominated by noise in the images of

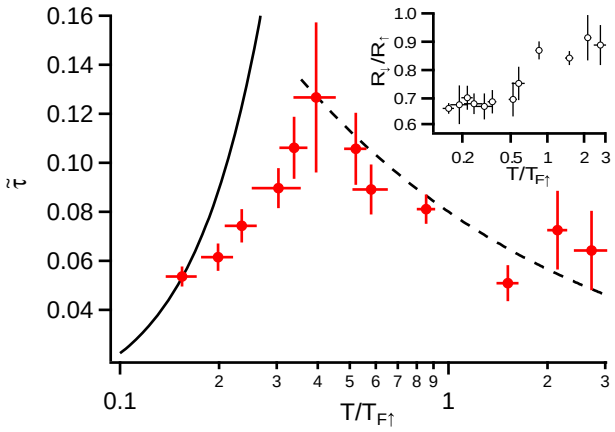


**Figure 2.** Normalized relaxation time of the spin-dipole mode of a highly polarized Fermi gas as a function of the reduced temperature $T/T_{\mathrm{F}\uparrow}$. $T_{\mathrm{F}\uparrow}$ is the local Fermi temperature at the center of the majority cloud. The solid curve is the low-temperature limit from [18], given by equation (7). The dashed curve is the expression $0.08\sqrt{\frac{T_{\mathrm{F}\uparrow}}{T}}$. The inset shows the average ratio of the minority cloud size to the majority cloud size as a function of the reduced temperature $T/T_{\mathrm{F}\uparrow}$. The cloud sizes are defined as the $1/e$ radii along the $z$-axis, estimated by fitting a 2D Gaussian function to the column densities of the two spin states. In both figures, each point is a weighted average of the results from 1 to 3 time series, with each time series containing on average 30 spin-up–spin-down image pairs. The error bars give standard deviations due to statistical fluctuations within a time series. Where the results of more than one time series are averaged, the error bars show the standard deviation of the weighted mean, determined from the standard deviations from each time series.

the clouds, giving an uncertainty in $w_0$ of about $2\,\mu$m. This implies a 7% systematic error on the potential energy at $\rho = 40\,\mu$m (a typical value of $\rho$ in the outer region of the cloud). The resulting systematic uncertainty on the temperature is 10% at the lowest temperatures, and 5% for temperatures near $T_{\mathrm{F}}$ or higher. Measurements of density are affected by the laser linewidth, imperfect polarization of the imaging light, and nonlinearities from saturation of the imaging transition, Doppler shifting of atoms scattered by the imaging light and pumping into transparent final states. The density measurement is calibrated using equilibrium low-temperature clouds with large spin imbalance. The systematic uncertainty in the density is 10%. This leads to a total systematic error in the reduced temperatures of 8–12%, and a systematic error in $\tilde{\tau}$ of 6%. The magnification of the imaging system is calibrated to 0.5% and does not contribute significantly to the uncertainties in $w_0$ or $d$.

It would be interesting to have available a calculation of spin transport coefficients such as $1/\tau_P$ at arbitrary temperatures for comparison with our data. A full solution is available for Fermi gases with equal populations in one spatial dimension [22, 23] and shows qualitative features similar to our data, with a maximum of the spin drag coefficient (analogous to $\tilde{\tau}$) at finite temperatures of the order of $T_{\mathrm{F}}$.

We expect our data to differ quantitatively from predictions for a homogeneous system. The measured quantity $\tilde{\tau}$ is a global property of the trapped system, while the momentum relaxation

rate $1/\tau_P$ is a local quantity. For $T \gg T_{F\uparrow}$, $1/\tau_P \propto n_\uparrow$, and $1/\tau_P$ increases with increasing majority density, while for $T \ll T_{F\uparrow}$, due to Pauli blocking $1/\tau_P \propto E_{F\uparrow}(T/T_{F\uparrow})^2 \propto n_\uparrow^{-2/3}$, and $1/\tau_P$ decreases with increasing majority density. Additionally, the variation in $1/\tau_P$ should cause the spin current to be non-uniform. The effect of inhomogeneity should be greater at high reduced temperatures, where the minority cloud size approaches the majority cloud size. The inset in figure 2 shows the ratio of the cloud sizes $R_\downarrow/R_\uparrow$ as a function of the reduced temperature, where $R_{\uparrow(\downarrow)}$ is the $1/e$ width in the $z$-direction from a 2D Gaussian fit to the majority (minority) column density. Indeed, $R_\downarrow/R_\uparrow$ increases with increasing $T/T_{F\uparrow}$. Even at the lowest temperatures, $R_\downarrow/R_\uparrow$ remains significant, attaining a value of 0.7, due to the finite minority fraction $N_\downarrow/N_\uparrow \approx 0.1$. The effect of inhomogeneity is therefore reduced at low temperatures, but should remain present.

We compare our results for $\tilde{\tau}$ at low temperatures to the low-temperature limit in [18], which can be written as

$$\frac{1/\tau_P(\mathbf{0})}{E_{F\uparrow}/\hbar} = c\frac{\alpha^2}{1+\alpha}\left(\frac{m^*}{m}\right)^2\left(\frac{T}{T_{F\uparrow}}\right)^2, \tag{7}$$

for temperatures $T \ll T_{F\uparrow}$.[3] The prefactor $c$ changes slightly from $c = \frac{2\pi^3}{9} = 6.89\ldots$ to c $\approx 6.0$ as the temperature rises from far below $T_{F\downarrow}$, where even the minority cloud is degenerate, to temperatures where $T_{F\downarrow} \ll T \ll T_{F\uparrow}$ and the minority is a classical gas [18]. In our coldest data, $T \approx 0.5T_{F\downarrow}$ and $T_{F\downarrow} \approx 0.3T_{F\uparrow}$, assuming $m^* = 1.2\,m$. To compare our data with [18], using (7), we set $c = \frac{2\pi^3}{9}$, $\alpha = 0.6$ and $m^* = 1.2\,m$. The comparison is affected by the inhomogeneous trapping potential in the experiment, as equation (7) gives the local value of $1/\tau_P$ at the center of the majority cloud. The experimental data agree with the value from equation (7) at the lowest temperatures measured (see figure 2). The deviation at higher temperatures is expected as the $T \ll T_{F\uparrow}$ limit becomes inapplicable. The convergence of the experimental data to the theoretical value at low temperature despite the inhomogeneity of the system may be partly due to the reduced minority cloud size at low temperatures, which reduces the effects of inhomogeneity, as discussed above. Additionally, the variation in the momentum relaxation rate with density will to some extent cancel at moderately low temperatures, as $1/\tau_P$ changes from increasing with increasing density at high reduced temperatures to decreasing with increasing density due to Pauli blocking at low reduced temperatures. The crossing of the experimental curve with the predictions for a uniform system at low temperatures therefore does not necessarily indicate that the inhomogeneity is negligible at low temperatures in this measurement.

At high temperatures $T \gg T_{F\uparrow,\downarrow}$, the spin transport properties of a trapped system can be calculated from the Boltzmann transport equation. For vanishing minority fraction, we find (now with $\alpha = 0$ and $m^* = m$ and assuming harmonic trapping in all three directions) [14]

$$\tilde{\tau} = \frac{8}{9\pi^{3/2}\epsilon}\sqrt{\frac{T_{F\uparrow}}{T}} \approx \frac{0.16}{\epsilon}\sqrt{\frac{T_{F\uparrow}}{T}}, \tag{8}$$

where $\epsilon = 1$ when the minority drift velocity distribution $v_\downarrow$ is uniform. This result features the expected dependence $\propto \sqrt{\frac{T_{F\uparrow}}{T}}$ on temperature. The relative velocity between the two spin states

[3] We omit a term due to the relative velocity of the spin up and spin-down clouds, which produces a correction of less than 1% in the overdamped, finite-temperature regime accessed in this experiment.

cannot be truly constant in space but has to be depressed in the center, where the density is highest and the momentum relaxation is fastest. In general,

$$\epsilon = \frac{\int \mathrm{d}^3 r\, v_\downarrow(\frac{\vec{r}}{\sqrt{2}})\mathrm{e}^{-\beta V}}{\int \mathrm{d}^3 r\, v_\downarrow(\vec{r})\mathrm{e}^{-\beta V}}, \tag{9}$$

where $V$ is the trapping potential (here assumed to be quadratic). For example, for a quadratic drift velocity profile, $v_\downarrow(\vec{r}) = ax^2 + by^2 + cz^2$, the predicted $\tilde{\tau}$ is reduced by factor of $\epsilon = 2$. We find that the high-temperature result (8) with $\epsilon = 2$ leads to close agreement with our experimental results (figure 2). This model is interesting because it estimates the effects of inhomogeneous density and velocity distributions, but it has shortcomings. The drift velocity should remain non-zero everywhere, rather than going to zero at the origin as in the quadratic case, and should have a radial component. A full quantitative description of the overdamped spin-dipole motion in the high-temperature limit in an external trapping potential will therefore be more complex.

### 3. A superfluid with small spin polarization

We extend the method of the previous section to study spin transport in Fermi gases with resonant interactions and small spin imbalance. When the global polarization $\frac{N_\uparrow - N_\downarrow}{N_\uparrow + N_\downarrow}$ is less than about 75% in a harmonically trapped Fermi gas at low temperature and with resonant interactions, the system phase separates into a superfluid core surrounded by a polarized normal state region [15, 16, 21]. The superfluid core is visible as a sharp reduction in the density difference of the two spin states [16]. The transition between the superfluid and the imbalanced normal regions forms a sharp interface below a tricritical point, where the density imbalance jumps between the two regions [39]. Scattering and spin transport at the interface between a normal and superfluid Fermi gas have been considered theoretically in [20, 41].

To observe spin transport in an imbalanced gas containing a superfluid, we prepare a spin mixture with a global polarization of 17(3)%. The gas is cooled at 300 G and again at 834 G after creating the spin-dipole excitation as described in the previous section. Two off-resonant phase contrast images are taken to measure the densities of each spin state. An imaging pulse tuned halfway between the resonance frequencies of the two states directly measures the difference in the column densities (figure 3(a)), while a second pulse, red-detuned from both states (figure 3(b)), provides additional information needed to reconstruct the total column density in each state [39]. From the column densities of each state, we obtain 3D density distributions using the inverse Abel transformation.

The 2D spin density (figure 3(a)) and 3D spin density (figure 3(c)) show a reduction near the center of the trap, with the 3D density going to zero, characteristic of the superfluid core in imbalanced Fermi gases [16]. We have checked that the shell structure remains even after the spin density reaches equilibrium. Additionally, we estimate the temperature $T$ of the system to confirm that it is cold enough to contain a superfluid. In unpolarized systems, the superfluid transition is predicted to occur at about $T_c/T_F = 0.173(6)$ [42], where $k_B T_F = E_F = \hbar^2(6\pi^2 n(0))^{2/3}/2m$ and $n$ is the density per spin state. This theoretical value agrees well with a determination of $T_c/T_F$ by our group. Fitting the equation of state of a unitary Fermi gas at zero imbalance [43] to the majority (minority) density gives an estimate $T_{\uparrow(\downarrow)}$ of the temperature. The fits are restricted to $V_{\sigma,\mathrm{eff}} > 0.3\,\mu$K, where $V_{\sigma,\mathrm{eff}} = V(\rho, z - Z_\sigma)$, to exclude

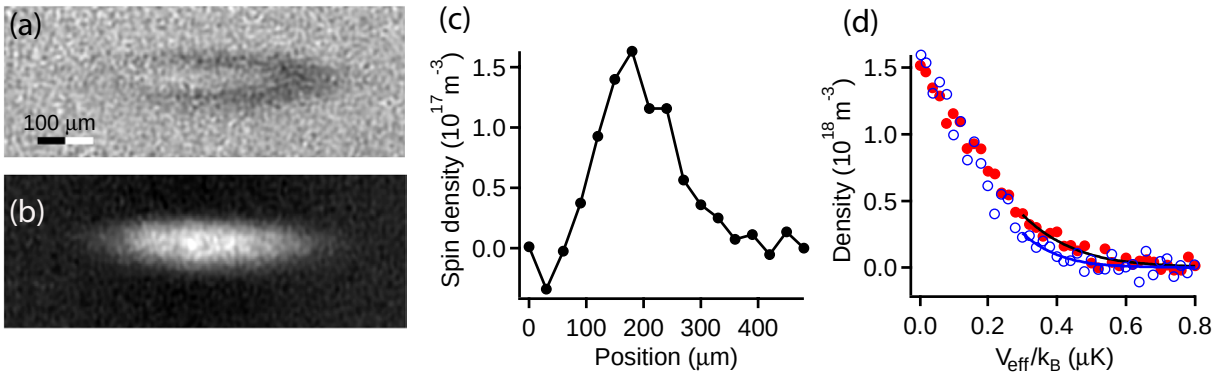


**Figure 3.** Spin-dipole mode of an imbalanced Fermi gas with a superfluid core. Phase contrast images are taken with imaging light detuned (a) halfway between the resonance frequencies of the two states and (b) at large red detuning from both states. The image in (a) is proportional to the difference in column densities of the two states. The depletion of the density difference in the center of the cloud indicates the superfluid region. It is displaced from the center of the majority due to the spin-dipole excitation. Panel (c) shows the difference in reconstructed 3D densities of the spin up and spin-down clouds as a function of the $z$ coordinate for $z > 0$. The depletion in the center again indicates pairing and superfluidity [16]. An elliptical average over a narrow range of the radial coordinate $\rho$ is used to increase the signal-to-noise ratio. (d) The temperature is estimated from the 3D densities of the two states as a function of the effective potential $V_{\mathrm{eff}}$ defined in the text. Solid red circles: majority density, open blue circles: minority density. The curves are fits to the densities using the equation of state of a unitary Fermi gas at zero imbalance to get upper and lower bounds on the temperature.

the putative superfluid region. Compared to a balanced gas at unitarity with $N'_\uparrow = N'_\downarrow = N_\uparrow$, and at the same temperature T, the majority cloud should have a larger size because the interaction energy between the spin-up and spin-down atoms is attractive. We therefore expect that $T_\uparrow$ is an overestimate of $T$. Likewise, we expect $T_\downarrow < T$, and we consider $T_\uparrow$ and $T_\downarrow$ to provide approximate upper and lower bounds on $T$.

Figure 4(a) shows the temperature bounds during the approach to equilibrium. Time-averaging gives $0.12(1) < T/T_{\mathrm{F}} < 0.15(2)$, where $T_{\mathrm{F}} \equiv T_{\mathrm{F}\uparrow} \approx T_{\mathrm{F}\downarrow}$. The error estimates include the standard error of the mean and the systematic error from uncertainty in the potential energy and in the density. These temperature bounds confirm that the system is in the vicinity of the superfluid transition.

Even in the presence of the superfluid core, we still observe strong damping of the spin-dipole mode. Figure 4(b) shows that the displacement $d$ between the majority and minority centers of mass along the $z$-axis relaxes gradually to zero, rather than oscillating as would be expected in a dissipationless system. The $1/e$ relaxation time $\tau = 360\,\mathrm{ms}$ corresponds to a spin drag coefficient [13, 22] of $\omega_z^2\tau = 0.06(1)E_{\mathrm{F}\uparrow}/\hbar$, close to the maximum spin drag coefficient in non-polarized trapped Fermi gases at unitarity [14].

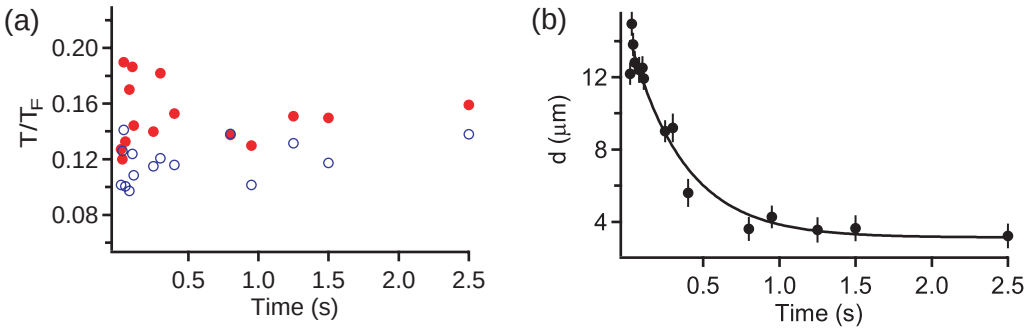


**Figure 4.** (a) Reduced temperature as a function of time during relaxation of the spin-dipole excitation in a spin-polarized Fermi gas containing a superfluid region. Red solid (blue open) circles: $T_{\uparrow(\downarrow)}/T_{F\uparrow(\downarrow)}$ from a fit to the edge of the majority (minority) spin state using the equation of state of an unpolarized unitary Fermi gas, giving an upper (lower) limit to true temperature. (b) The displacement of the spin-up and spin-down centers of mass relaxes exponentially, indicating strong spin drag despite the presence of a superfluid. Error bars: one std. dev. from fitting error.

The strong damping is reminiscent of the friction between the normal and superfluid component in liquid helium [44] and in atomic Bose–Einstein condensates [46]. In the latter case, out-of-phase oscillations between the condensate and the thermal component are strongly damped. Even at low temperatures, currents in superfluids as well as in 1D superconducting wires are still damped due to phase slips [46–48]. In the presented case of a partially polarized Fermi gas, Andreev reflection of unpaired atoms at the normal-to-superfluid interface should cause spin current decay even at the lowest temperatures [20, 41]. At higher temperatures or if the majority chemical potential in the normal state region can overcome the pairing gap, the microscopic velocity of majority atoms will significantly exceed the critical velocity of the superfluid of about $0.3v_F$ [49, 50], causing strong dissipation of spin currents. The relative importance of dissipation at the interface versus dissipation inside the superfluid could be determined by whether a spin current flows through the superfluid or around it. However, we are not able to determine the spatial distribution of the spin current with our current data.

## 4. Conclusions

In this work, we presented our measurements on the damping of the spin-dipole mode in a highly polarized Fermi gas with resonant interactions, over a wide range of temperatures. The damping is seen to become weaker at temperatures significantly less than the majority Fermi energy, as expected from Pauli blocking, i.e. the fact that quasi-particles in a Fermi liquid become long lived at sufficiently low temperatures. These measurements provide the first quantitative test of theoretical calculations of the spin transport properties of highly polarized Fermi gases. We also observe spin transport in a Fermi gas with low spin polarization containing a superfluid region. It is found that the spin-dipole motion remains strongly damped, revealing the importance of friction between the superfluid and the normal component, possibly accompanied by reflection processes at the interface.

## Acknowledgments

This work was supported by the NSF, AFOSR-MURI, AFOSR-YIP, ARO-MURI, ONR, DARPA YFA, a grant from the Army Research Office with funding from the DARPA OLE program, the David and Lucille Packard Foundation and the Alfred P Sloan Foundation. The authors thank André Schirotzek, Giacomo Roati and Peyman Ahmadi for experimental assistance and David Huse for interesting discussions.

## References

[1] Chin C, Grimm R, Julienne P and Tiesinga E 2010 Feshbach resonances in ultracold gases *Rev. Mod. Phys.* **82** 1225–86
[2] Ketterle W and Zwierlein M W 2008 Making, probing and understanding ultracold Fermi gases *Ultracold Fermi Gases, Proc. Int. School of Physics 'Enrico Fermi', Course CLXIV (Varenna, 20–30 June 2006)* ed M Inguscio, W Ketterle and C Salomon (Amsterdam: IOS Press) pp 1–462
[3] Giorgini S, Pitaevskii L P and Stringari S 2008 Theory of ultracold atomic Fermi gases *Rev. Mod. Phys.* **80** 1215–60
[4] Cao C, Elliott E, Joseph J, Wu H, Petricka J, Schäfer T and Thomas J E 2010 Universal quantum viscosity in a unitary Fermi gas *Science* **331** 58–61
[5] O'Hara K M, Hemmer S L, Gehm M E, Granade S R and Thomas J E 2002 Observation of a strongly interacting degenerate Fermi gas of atoms *Science* **298** 2179
[6] Kinast J, Hemmer S L, Gehm M E, Turlapov A and Thomas J E 2004 Evidence for superfluidity in a resonantly interacting Fermi gas *Phys. Rev. Lett.* **92** 150402
[7] Bartenstein M, Altmeyer A, Riedl S, Jochim S, Chin C, Hecker-Denschlag J and Grimm R 2004 Collective excitations of a degenerate gas at the BEC-BCS crossover *Phys. Rev. Lett.* **92** 203201
[8] Altmeyer A, Riedl S, Kohstall C, Wright M J, Geursen R, Bartenstein M, Chin C, Hecker J Denschlag and Grimm R 2007 Precision measurements of collective oscillations in the BEC-BCS crossover *Phys. Rev. Lett.* **98** 040401
[9] Zwierlein M W, Abo-Shaeer J R, Schirotzek A, Schunck C H and Ketterle W 2005 Vortices and superfluidity in a strongly interacting Fermi gas *Nature* **435** 1047–51
[10] DeMarco B and Jin D S 2002 Spin excitations in a Fermi gas of atoms *Phys. Rev. Lett.* **88** 040405
[11] Gensemer S D and Jin D S 2001 Transition from collisionless to hydrodynamic behavior in an ultracold Fermi gas *Phys. Rev. Lett.* **87** 173201
[12] Du X, Luo L, Clancy B and Thomas J E 2008 Observation of anomalous spin segregation in a trapped Fermi gas *Phys. Rev. Lett.* **101** 150401
[13] D'Amico I and Vignale G 2000 Theory of spin Coulomb drag in spin-polarized transport *Phys. Rev.* B **62** 4853–7
[14] Sommer A, Ku M, Roati G and Zwierlein M W 2011 Universal spin transport in a strongly interacting Fermi gas *Nature* **472** 201–4
[15] Zwierlein M W, Schirotzek A, Schunck C H and Ketterle W 2006 Fermionic superfluidity with imbalanced spin populations *Science* **311** 492–6
[16] Shin Y, Zwierlein M W, Schunck C H, Schirotzek A and Ketterle W 2006 Observation of phase separation in a strongly interacting imbalanced Fermi gas *Phys. Rev. Lett.* **97** 030401
[17] Schirotzek A, Wu C-H, Sommer A and Zwierlein M W 2009 Observation of Fermi polarons in a tunable Fermi liquid of ultracold atoms *Phys. Rev. Lett.* **102** 230402–4
[18] Bruun G M, Recati A, Petchick C J, Smith H and Stringari S 2008 Collisional properties of a polarized Fermi gas with resonant interactions *Phys. Rev. Lett.* **100** 240406
[19] Recati A, Lobo C and Stringari S 2008 Role of interactions in spin-polarized atomic Fermi gases at unitarity *Phys. Rev.* A **78** 023633

[20] Parish M M and Huse D A 2009 Evaporative depolarization and spin transport in a unitary trapped Fermi gas *Phys. Rev.* A **80** 063605
[21] Nascimbène S, Navon N, Jiang K J, Tarruell L, Teichmann M, McKeever J, Chevy F and Salomon C 2009 Collective oscillations of an imbalanced Fermi gas: axial compression modes and polaron effective mass *Phys. Rev. Lett.* **103** 170402–4
[22] Polini M and Vignale G 2007 Spin drag and spin-charge separation in cold Fermi gases *Phys. Rev. Lett.* **98** 266403
[23] Rainis D, Polini M, Tosi M P and Vignale G 2008 Spin-drag relaxation time in one-dimensional spin-polarized Fermi gases *Phys. Rev.* B **77** 035113
[24] Duine R A, Polini M, Stoof H T C and Vignale G 2010 Spin drag in an ultracold Fermi gas on the verge of ferromagnetic instability *Phys. Rev. Lett.* **104** 220403
[25] Clogston A M 1962 Upper limit for the critical field in hard superconductors *Phys. Rev. Lett.* **9** 266
[26] Chandrasekhar B S 1962 A note on the maximum critical field of high-field superconductors *Appl. Phys. Lett.* **1** 7
[27] Chevy F 2006 Universal phase diagram of a strongly interacting Fermi gas with unbalanced spin populations *Phys. Rev.* A **74** 063628
[28] Combescot R, Recati A, Lobo C and Chevy F 2007 Normal state of highly polarized Fermi gases: simple many-body approaches *Phys. Rev. Lett.* **98** 180402
[29] Prokof'ev N and Svistunov B 2008 Fermi-polaron problem: diagrammatic Monte Carlo method for divergent sign-alternating series *Phys. Rev.* B **77** 020408
[30] Lobo C, Recati A, Giorgini S and Stringari S 2006 Normal state of a polarized Fermi gas at unitarity *Phys. Rev. Lett.* **97** 200403
[31] Shin Y-I 2008 Determination of the equation of state of a polarized Fermi gas at unitarity *Phys. Rev.* A **77** 041603
[32] Nascimbène S, Navon N, Jiang K J, Chevy F and Salomon C 2010 Exploring the thermodynamics of a universal Fermi gas *Nature* **463** 1057–60
[33] Combescot R and Giraud S 2008 Normal state of highly polarized Fermi gases: full many-body treatment *Phys. Rev. Lett.* **101** 050404
[34] Prokof'ev N V and Svistunov B V 2008 Bold diagrammatic Monte Carlo: a generic sign-problem tolerant technique for polaron models and possibly interacting many-body problems *Phys. Rev.* B **77** 125101
[35] Pilati S and Giorgini S 2008 Phase separation in a polarized Fermi gas at zero temperature *Phys. Rev. Lett.* **100** 030401
[36] Hadzibabic Z, Gupta S, Stan C A, Schunck C H, Zwierlein M W, Dieckmann K and Ketterle W 2003 Fifty-fold improvement in the number of quantum degenerate fermionic atoms *Phys. Rev. Lett.* **91** 160401
[37] Zwierlein M W, Schunck C H, Schirotzek A and Ketterle W 2006 Direct observation of the superfluid phase transition in ultracold Fermi gases *Nature* **442** 54–8
[38] Dobson J F 1994 Harmonic-potential theorem: implications for approximate many-body theories *Phys. Rev. Lett.* **73** 2244
[39] Shin Y-I, Schunck C H, Schirotzek A and Ketterle W 2008 Phase diagram of a two-component Fermi gas with resonant interactions *Nature* **451** 689–93
[40] Vichi L and Stringari S 1999 Collective oscillations of an interacting trapped Fermi gas *Phys. Rev.* A **60** 4734
[41] Van Schaeybroeck B and Lazarides A 2007 Normal-superfluid interface scattering for polarized fermion gases *Phys. Rev. Lett.* **98** 170402
[42] Goulko O and Wingate M 2010 Thermodynamics of balanced and slightly spin-imbalanced Fermi gases at unitarity *Phys. Rev.* A **82** 053621
[43] Ku M, Schirotzek A, Sommer A, Zwierlein M, Van K Houcke, Werner F, Kozik E, Prokofev N and Svistunov B 2010 equation of state of a strongly interacting atomic Fermi gas, available at http://meetings.aps.org/link/BAPS.2010.DAMOP.W6.1
[44] Vinen W F 1957 Mutual friction in a heat current in liquid helium ii. iii theory of mutual friction *Proc. R. Soc.* A **242** 493–515

[45] Stamper-Kurn D M, Miesner H-J, Inouye S, Andrews M R and Ketterle W 1998 Collisionless and hydrodynamic excitations of a Bose–Einstein condensate *Phys. Rev. Lett.* **81** 500–3
[46] Langer J S and Michael Fisher E 1967 Intrinsic critical velocity of a superfluid *Phys. Rev. Lett.* **19** 560–3
[47] Langer J S and Ambegaokar V 1967 Intrinsic resistive transition in narrow superconducting channels *Phys. Rev.* **164** 498–510
[48] McKay D, White M, Pasienski M and DeMarco B 2008 Phase-slip-induced dissipation in an atomic Bose–Hubbard system *Nature* **453** 76–80
[49] Miller D E, Chin J K, Stan C A, Liu Y, Setiawan W, Sanner C and Ketterle W 2007 Critical velocity for superfluid flow across the BEC-BCS crossover *Phys. Rev. Lett.* **99** 070402
[50] Combescot R, Kagan M Yu and Stringari S 2006 Collective mode of homogeneous superfluid Fermi gases in the BEC-BCS crossover *Phys. Rev.* A **74** 042717

LETTER

doi:10.1038/nature09989

# Universal spin transport in a strongly interacting Fermi gas

Ariel Sommer[1,2,3], Mark Ku[1,2,3], Giacomo Roati[4,5] & Martin W. Zwierlein[1,2,3]

**Transport of fermions, particles with half-integer spin, is central to many fields of physics. Electron transport runs modern technology, defining states of matter such as superconductors and insulators, and electron spin is being explored as a new carrier of information[1]. Neutrino transport energizes supernova explosions following the collapse of a dying star[2], and hydrodynamic transport of the quark–gluon plasma governed the expansion of the early Universe[3]. However, our understanding of non-equilibrium dynamics in such strongly interacting fermionic matter is still limited. Ultracold gases of fermionic atoms realize a pristine model for such systems and can be studied in real time with the precision of atomic physics[4]. Even above the superfluid transition, such gases flow as an almost perfect fluid with very low viscosity when interactions are tuned to a scattering resonance[3,5–8]. In this hydrodynamic regime, collective density excitations are weakly damped[6,7]. Here we experimentally investigate spin excitations in a Fermi gas of $^6$Li atoms, finding that, in contrast, they are maximally damped. A spin current is induced by spatially separating two spin components and observing their evolution in an external trapping potential. We demonstrate that interactions can be strong enough to reverse spin currents, with components of opposite spin reflecting off each other. Near equilibrium, we obtain the spin drag coefficient, the spin diffusivity and the spin susceptibility as a function of temperature on resonance and show that they obey universal laws at high temperatures. In the degenerate regime, the spin diffusivity approaches a value set by $\hbar/m$, the quantum limit of diffusion, where $\hbar$ is Planck's constant divided by $2\pi$ and $m$ the atomic mass. For repulsive interactions, our measurements seem to exclude a metastable ferromagnetic state[9–11].**

Understanding the transport of spin, as opposed to the transport of charge, is highly relevant to the novel field of spintronics[1]. Whereas charge currents are unaffected by electron–electron scattering owing to momentum conservation, spin currents are intrinsically damped owing to collisions between electrons of opposite spin, as their relative momentum is not conserved. This phenomenon is known as spin drag[12,13]. It is expected to contribute significantly to the damping of spin currents in doped semiconductors[14]. The random collision events also lead to spin diffusion—the tendency for spin currents to flow in such a way as to even out spatial gradients in the spin density—which has been studied in high-temperature superconductors[15] and in liquid $^3$He–$^4$He mixtures[16,17].

Creating spin currents poses a major challenge in electronic systems, where mobile spins are scattered by their environment and by each other. However, in ultracold atomic gases, we have the freedom to first prepare an essentially non-interacting spin mixture, separate atoms spatially by using magnetic field gradients, and only then induce strong interactions. Past observations of spin currents in ultracold Fermi gases[18,19] were made in the weakly interacting regime. Here we access the regime near a Feshbach resonance[4], where interactions are as strong as allowed by quantum mechanics (the unitarity limit). We measure spin transport properties, namely the spin drag coefficient $\Gamma_{\mathrm{sd}}$ and the spin diffusivity $D_{\mathrm{s}}$, of a strongly interacting Fermi gas composed of an equal number of atoms in two different spin states. In the strongly interacting regime, spin drag is expected to reach a universal maximum value, and spin diffusion is expected to reach a universal minimum.

The universal behaviour of the spin transport coefficients of a Fermi gas can be estimated on general grounds. At the Feshbach resonance, the scattering cross-section $\sigma$ between atoms of opposite spin is given by the square of the de Broglie wavelength. In the degenerate regime (that is, below the Fermi temperature $T_{\mathrm{F}}$) $\sigma \approx 1/k_{\mathrm{F}}^2$, where $k_{\mathrm{F}} = (6\pi^2 n)^{1/3}$ is the Fermi wavevector and $n$ is the density of atoms in each spin state. The mean free path between collisions is thus $l = 1/(n\sigma) \approx 1/k_{\mathrm{F}}$, or about one interparticle spacing, which is the smallest possible mean free path in a gas. The average speed $v$ of atoms is of the order of the Fermi velocity, $\hbar k_{\mathrm{F}}/m$. In estimating the spin diffusivity $D_{\mathrm{s}} \approx vl$, the density-dependent factors cancel, giving $D_{\mathrm{s}} \approx \hbar/m$. This value for $D_{\mathrm{s}}$ represents a universal quantum limit to spin diffusivity in Fermi gases. Away from resonance, the scattering cross-section decreases, increasing $D_{\mathrm{s}}$. For temperatures $T$ much greater than $T_{\mathrm{F}}$, the scattering cross-section will be given by the square of the thermal de Broglie wavelength, and thus decreases as $\sigma \propto 1/T$. The velocity, in turn, will increase as $v \propto \sqrt{T}$, causing $D_{\mathrm{s}}$ to increase as $D_{\mathrm{s}} \propto T^{3/2}$. An analogous scaling argument applies to the viscosity[7,8]. Finally, in a degenerate Fermi gas, the average velocity will remain of the order of the Fermi velocity, but the effective scattering cross-section will scale as $\sigma \propto T^2$ owing to Pauli blocking, causing $D_{\mathrm{s}}$ to increase as $T^{-2}$ as the temperature is lowered. For a Fermi gas, we thus expect the minimum $D_{\mathrm{s}}$ to occur near $T_{\mathrm{F}}$, before Pauli blocking becomes effective. Correspondingly, the coefficient $\Gamma_{\mathrm{sd}}$ characterizing spin drag is expected to reach a universal maximum value, given by the Fermi rate $E_{\mathrm{F}}/h$, where $E_{\mathrm{F}} = \hbar^2 k_{\mathrm{F}}^2/2m$ is the Fermi energy.

In our experiment, we prepare an equal mixture of the two lowest hyperfine states ('spin up' and 'spin down') of fermionic $^6$Li in a cylindrically symmetric atom trap[4,20,21]. The confinement along the axis of symmetry is harmonic, with frequency $\omega_z$. We separate the two spin components along the axis of symmetry of the trap (see Methods Summary), and turn on strong interactions between unequal spins by quickly increasing the magnetic field to a Feshbach resonance located at 834 G. The confining potential of the trap forces the two clouds of opposite-spin atoms to propagate towards each other, establishing a spin current. Measurements are made by selectively imaging the two spin components.

Figure 1 shows the collision between the two spin domains on resonance. The clouds bounce off each other and essentially completely repel each other. Owing to the axial trapping potential, the clouds return after the collision, and we observe several oscillations in the displacement $d = \langle z_\uparrow \rangle - \langle z_\downarrow \rangle$, where $\langle z_{\uparrow(\downarrow)} \rangle$ is the centre of mass of the spin-up (spin-down) cloud. After the oscillations have decayed, the displacement decreases to zero monotonically, on a timescale of the

[1]Department of Physics, Massachusetts Institute of Technology, Cambridge, Massachusetts 02139, USA. [2]MIT-Harvard Center for Ultracold Atoms, Massachusetts Institute of Technology, Cambridge, Massachusetts 02139, USA. [3]Research Laboratory of Electronics, Massachusetts Institute of Technology, Cambridge, Massachusetts 02139, USA. [4]INO-CNR, University of Florence, 50019 Sesto Fiorentino, Italy. [5]LENS, University of Florence, 50019 Sesto Fiorentino, Italy.

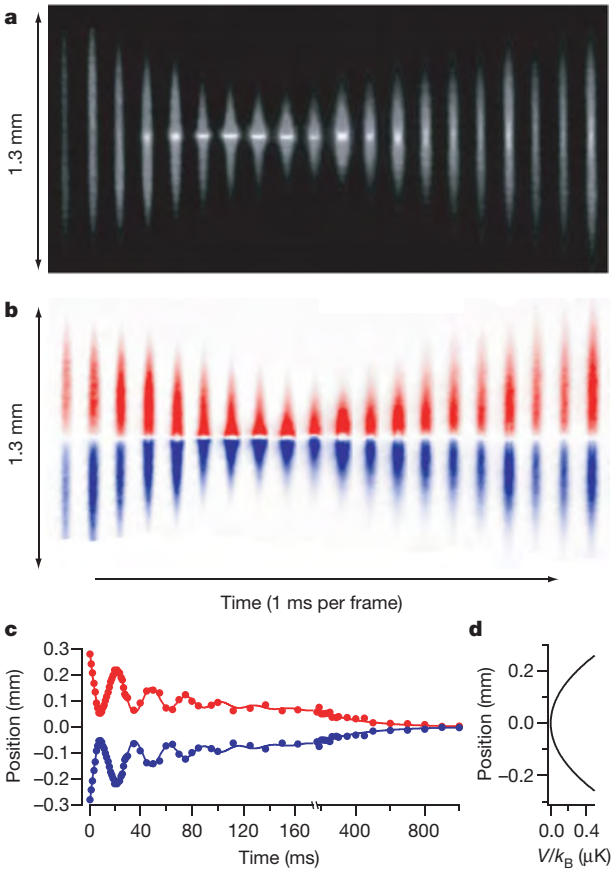


**Figure 1 | Observation of spin current reversal in a resonant collision between two oppositely spin-polarized clouds of fermions.** **a**, **b**, Total column density (**a**) and the difference in column densities (**b**: red, spin up; blue, spin down) during the first 20 ms after the collision. The central column densities here are typically $7 \times 10^9$ cm$^{-2}$. Strong repulsion is observed that leads to a high-density interface. **c**, The centre of mass separation initially oscillates at 1.63(2) times the axial trap frequency of 22.8 Hz (see Supplementary Information) before decaying exponentially at later times. The initial atom number per spin state is $1.2 \times 10^6$, and the temperature 200 ms after the collision and later is $0.5T_F$, with $T_F$ the Fermi temperature at the centre of each cloud. **d**, The trapping potential $V$ is harmonic along the symmetry axis.

order of one second, which is an extremely long time compared to the trapping period (44 ms). The underlying explanation for spin current reversal and the slow relaxation can be found in the extremely short mean free path and the high collision rate between opposite-spin atoms at unitarity. According to the above estimate, the spin diffusivity is approximately $\hbar/m$, which for $^6$Li is (100 μm)$^2$ s$^{-1}$. The atom clouds in the experiment have a length of the order of 100 μm, and it takes them of the order of a second to diffuse through each other. So we are indeed observing quantum-limited spin diffusion. The initial bounces will occur when the mean free path of a spin-up atom in the spin-down cloud is smaller than the spin-down cloud size, that is, when the mixture is hydrodynamic. Instead of quickly diffusing into the spin-down region, it is then more likely that the spin-up atom is scattered back into the spin-up region, where it can propagate ballistically.

After long evolution times, the oscillations shown in Fig. 1 have been damped out, and the displacement between the centres of mass is much smaller than the widths of the clouds. The relaxation dynamics can then be described by linear response theory, giving access to the spin transport coefficients. The spin drag coefficient $\Gamma_{sd}$ is defined as the rate of momentum transfer between opposite-spin atoms[12,14], and is therefore related to the collision rate. From the Boltzmann transport equation, the relaxation of the displacement $d$ near equilibrium follows the differential equation[22]

$$\Gamma_{sd}\dot{d} + \omega_z^2 d = 0$$

in the case of strongly overdamped motion realized here. Fitting an exponential with decay time $\tau$ to the displacement gives the spin drag coefficient of the trapped system as $\Gamma_{sd} = \omega_z^2\tau$. In the deeply degenerate regime, the relationship between the measured and the microscopic spin drag coefficient might be affected by a weak enhancement of the effective mass[23] and the attractive interaction energy between the clouds[10,22,24].

The spin drag coefficient is found to be greatest on resonance, and thus spin conduction is slowest on resonance (see Supplementary Information). On resonance, $\Gamma_{sd}$ in a homogeneous system must be given by a function of the reduced temperature $T/T_F$ times the Fermi rate $E_F/\hbar$. At high temperatures, we expect the spin drag coefficient to obey a universal scaling $\Gamma_{sd} \propto n\sigma v \propto \frac{E_F}{\hbar}(T/T_F)^{-1/2}$. In Fig. 2 we show the spin drag coefficient as a function of $T/T_F$; $\Gamma_{sd}$ is normalized by $E_F/\hbar$, where $E_F$ and $T_F$ are the local values at the centre of total mass. We observe $T^{-1/2}$ scaling for $T/T_F > 2$, finding $\Gamma_{sd} = 0.16(1)\frac{E_F}{\hbar}(T/T_F)^{-1/2}$. At lower temperatures, we observe a crossover from classical to non-classical behaviour as the spin drag coefficient reaches a maximum of approximately $0.1E_F/\hbar$ near the Fermi temperature. We interpret this saturation of the spin drag coefficient as a consequence of Fermi statistics and unitarity[4,5], as $\sigma$ and $v$ approach values determined by the Fermi wavevector $k_F$. The spin drag coefficient is inversely proportional to the spin conductivity, which describes the spin current response to an external spin-dependent force. Near the Fermi temperature, the maximum spin drag coefficient corresponds to a minimum spin conductivity of the order of $k_F/\hbar$. This is the slowest spin conduction possible in three dimensions in the absence of localization.

At low temperatures, the spin drag coefficient decreases with decreasing temperature. Reduced spin drag at low temperatures is expected in Fermi liquids owing to Pauli blocking[11,18,22,24,25], and is also expected in one-dimensional Fermi gases[26]. In the case of collective density (rather than spin) excitations, it was shown that pairing correlations enhance the effective collision rate dramatically as the temperature is lowered[6]. The effect of pairing on the spin drag coefficient may be qualitatively different. In a simple picture, spin currents require the flow of unpaired atoms, whereas collective density excitations affect paired and unpaired atoms alike.

Comparing the relaxation rate to the gradient in spin density allows us to also measure the spin diffusivity $D_s$. At the centre of the trap, the spin current density $J_s$ is given by the spin diffusion equation[27]

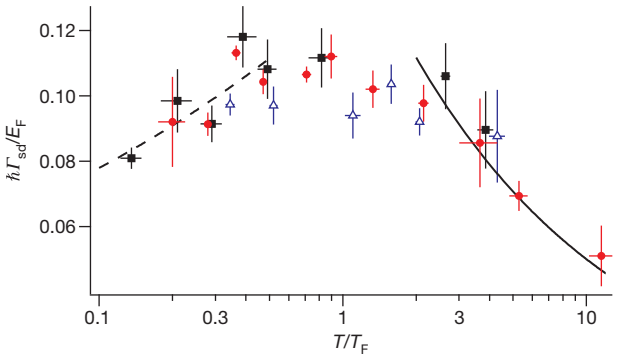


**Figure 2 | Spin drag coefficient of a trapped Fermi gas with resonant interactions.** The spin drag coefficient $\Gamma_{sd}$ is normalized by the Fermi rate $E_F/\hbar$ at the trap centre, whereas the temperature is normalized by $T_F = E_F/k_B$. We find agreement between measurements taken at three different axial trapping frequencies, 22.8 Hz (red circles), 37.5 Hz (blue triangles) and 11.2 Hz (black squares). The data for $T/T_F > 2$ fit to a $T^{-1/2}$ law (solid line). Dashed line, a power law fit for $T/T_F < 0.5$ to show the trend. Each point is a mean from typically three determinations of $\Gamma_{sd}$, each obtained from a time series of about 30 experimental runs and weighted according to the standard deviation from fitting error and shot to shot fluctuations. Error bars, ±1s.e.

$$J_s = -D_s \frac{\partial(n_\uparrow - n_\downarrow)}{\partial_z}$$

where $n_{\uparrow(\downarrow)}$ is the density of spin-up (spin-down) atoms. We calculate $J_s$ using the trap-averaged velocity as $J_s = \frac{1}{2}(n_\uparrow + n_\downarrow)\dot{d}$, where the densities are evaluated at the centre of total mass.

We find that the spin diffusivity is at a minimum when interactions are resonant (see Supplementary Information). The increase in spin diffusivity for positive scattering length $a$, as well as the decrease in spin drag, argues against the existence of a ferromagnetic state in repulsive Fermi gases, for which diffusion should stop entirely[9,11]. Figure 3 reports the measured spin diffusivity as a function of temperature at unitarity. In the high-temperature limit on resonance, one expects $D_s \propto v/n\sigma \propto T^{3/2}$. At high temperatures, we indeed find this temperature dependence, with a fit giving $D_s = 5.8(2)\frac{\hbar}{m}(T/T_F)^{3/2}$ for $T/T_F > 2$. In the degenerate regime, the spin diffusivity is seen to attain a limiting value of $6.3(3)\hbar/m$.

When comparing these results to theoretical calculations, it is important to account for the inhomogeneous density distributions and velocity profiles. For a homogeneous system on resonance, and at high temperatures compared to the Fermi temperature, we predict $D_s = 1.11\frac{\hbar}{m}(T/T_F)^{3/2}$ and $\Gamma_{sd} = 0.90\frac{E_F}{\hbar}(T/T_F)^{-1/2}$ (see Supplementary Information). The measured spin drag coefficient is smaller by a factor of 0.90/0.16(1) = 5.6(4) while the spin diffusivity is larger by about the same factor, 5.8(2)/1.11 = 5.3(2), compared to a homogeneous system at the density of the centre of total mass. These factors reflect the inhomogeneity of the system and agree with an estimate from the Boltzmann transport equation (see Supplementary Information). The emergence of a superfluid core at our lowest temperatures will further modify the ratio of trap-averaged to local transport coefficients.

Finally, the measured transport coefficients give for the first time access to the temperature dependence of the spin susceptibility, $\chi_s(T)$, in strongly interacting Fermi gases. Defined as $\chi_s = \frac{\partial(n_\uparrow - n_\downarrow)}{\partial(\mu_\uparrow - \mu_\downarrow)}$, the spin susceptibility describes the spin response to an infinitesimal effective magnetic field or chemical potential difference $\mu_\uparrow - \mu_\downarrow$ applied to the gas, and is a crucial quantity that can discriminate between different states of matter[10]. In a magnetic field gradient, particles with opposite spin are forced apart at a rate determined by the spin conductivity $\sigma_s$, while diffusion acts to recombine them. The balance between the processes of diffusion and conduction therefore determines the resulting magnetization gradient, a connection expressed in the Einstein relation[11] $\chi_s = \sigma_s/D_s$. Assuming the standard relation[11,14] $\sigma_s = n/(m\Gamma_{sd})$,

$$\chi_s = \frac{1}{md\omega_z^2}\frac{\partial(n_\uparrow - n_\downarrow)}{\partial z}$$

where $\frac{\partial(n_\uparrow - n_\downarrow)}{\partial z}$ is evaluated near the trap centre. The inhomogeneous trapping potential does not affect the measurement of $\chi_s$ in the hydrodynamic limit at high temperatures (see Supplementary Information). Close to the transition to superfluidity, interaction effects may modify the relation between $\sigma_s$ and $\Gamma_{sd}$.

Figure 4 reports our findings for the spin susceptibility at unitarity, as a function of the dimensionless temperature $T/T_F$. At high temperatures, we observe the Curie law $\chi_s = n/(k_B T)$, where $k_B$ is Boltzmann's constant. In this classical regime of uncorrelated spins, the susceptibility equals the (normalized) compressibility of the gas $n^2\kappa = \partial n/\partial\mu$ that we also directly obtain from our profiles. At degenerate temperatures, the measured spin susceptibility becomes smaller than the normalized compressibility. This is expected for a Fermi liquid, where $\chi_s = \frac{3n}{2E_F}\frac{1}{1+F_0^a}$ and $\kappa = \frac{3}{2nE_F}\frac{1}{1+F_0^s}$ with Landau parameters $F_0^s$ and $F_0^a$ describing the density (s) and spin (a) response[10]. The spin susceptibility is expected to strongly decrease at sufficiently low temperatures in the superfluid phase, as pairs will form that will not break in the presence of an infinitesimal magnetic field. It is currently debated whether the strongly interacting Fermi gas above the superfluid transition temperature is a Fermi liquid[23] or a state with an excitation gap (pseudogap)[28,29]. The opening of a gap in the excitation spectrum would be revealed as a downturn of the spin susceptibility below a certain temperature. Such a downturn is not observed in $\chi_s$ down to $T/T_F \approx 0.2$, and therefore our spin susceptibility data agree down to this point with the expected behaviour for a Fermi liquid.

In conclusion, we have studied spin transport in strongly interacting Fermi gases. The spin diffusivity was found to attain a limiting value of about $6.3\hbar/m$, establishing the quantum limit of diffusion for strongly interacting Fermi gases. Away from resonance, the diffusivity increases.

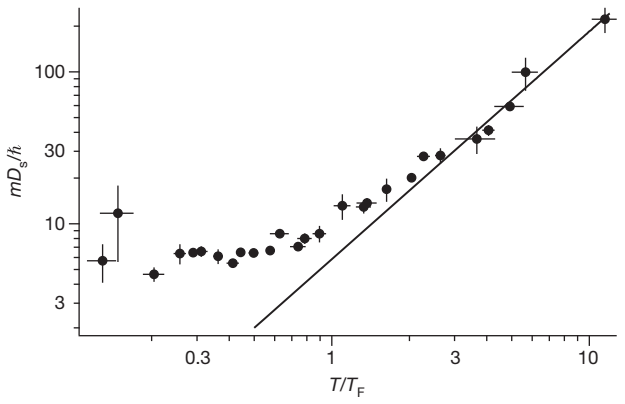


**Figure 3 | Spin diffusivity of a trapped Fermi gas.** Shown is the spin diffusivity on resonance ($D_s$, normalized by $\hbar/m$; filled circles) as a function of the dimensionless temperature $T/T_F$. At high temperatures, $D_s$ obeys the universal $T^{3/2}$ behaviour (solid line). At low temperatures, $D_s$ approaches a constant value of $6.3(3)\hbar/m$ for temperatures below about $0.5T_F$, establishing the quantum limit of spin diffusion for strongly interacting Fermi gases. Error bars, ±1s.e.

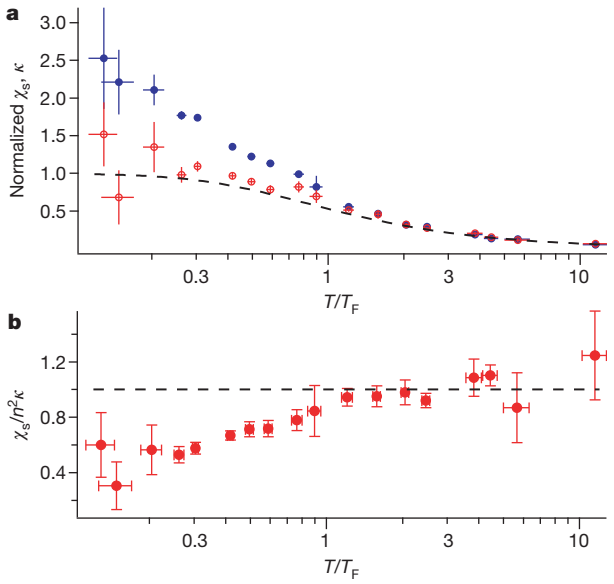


**Figure 4 | Spin susceptibility on resonance.** **a**, Spin susceptibility ($\chi_s$, open red circles) and isothermal compressibility ($\kappa$, filled blue circles), normalized by the values for an ideal Fermi gas at zero temperature. For temperatures below $T_F$, $\chi_s$ becomes suppressed relative to $\kappa$, owing to interactions between opposite-spin atoms. Dashed line, $\chi_s$ of a non-interacting Fermi gas for comparison. **b**, Red circles, $\chi_s$ divided by the value of $n^2\kappa$ obtained from the same clouds. At temperatures above $T_F$, the ratio of $\chi_s$ to $n^2\kappa$ approaches unity (dashed line). Error bars, ±1s.e.

This casts doubt on the possibility of stabilizing a ferromagnetic gas on the repulsive side of the Feshbach resonance[9], which would require a vanishing diffusivity[11]. The observed slow relaxation of spin excitations is a likely explanation for the surprising—possibly non-equilibrium[27]—profiles in spin-imbalanced Fermi gases reported in ref. 30, which did not agree with equilibrium measurements by other workers[20,21,31]. Our measurements of the temperature dependence of the spin susceptibility are consistent with a Fermi liquid picture, and do not reveal a pseudogap. An interesting subject for further study is whether spins are still able to diffuse through the superfluid, or whether they travel around it, avoiding the superfluid owing to the pairing gap.

## METHODS SUMMARY

The spin mixture is initially prepared at 300 G. To separate the spin components, we reduce the magnetic field to 50 G, where the magnetic moments of the two spin states are unequal, and apply two magnetic field gradient pulses. We then bring the total magnetic field to the Feshbach resonance in about 2 ms.

To reach low temperatures during the approach to equilibrium, evaporative cooling is applied, at 834 G, by gradually lowering the depth of the optical dipole trap. To reach high temperatures, we heat the atoms by switching off the optical dipole trap for up to 3 ms to allow the atom clouds to expand before recapturing them. We then set the final depth of the dipole trap so that the atom number and the temperature remain nearly constant during the approach to equilibrium.

Spin selective imaging is performed by means of *in situ* absorption or phase contrast imaging using two 4-μs imaging pulses separated by 6 μs. These images give the column densities of each spin state, from which we obtain the three-dimensional densities by way of an inverse Abel transform[21]. The gradient in the spin density is obtained from a linear fit to the polarization versus $z$.

We determine the temperature of the clouds by fitting the density versus potential energy in the vicinity of $z = 0$ (but for all values of the radial coordinate $r$) to the equation of state of the unitary Fermi gas, measured recently by our group[32]. The trapping potential itself is determined by summing the densities of hundreds of clouds, using the known axial, harmonic trapping potential to convert equidensity lines to equipotential lines and fitting the result to an analytic model.

**Received 4 January; accepted 4 March 2011.**


1. Wolf, S. A. Spintronics: a spin-based electronics vision for the future. *Science* **294,** 1488–1495 (2001).
2. Burrows, A. Neutrinos from supernova explosions. *Annu. Rev. Nucl. Part. Sci.* **40,** 181–212 (1990).
3. Schäfer, T. & Teaney, D. Nearly perfect fluidity: from cold atomic gases to hot quark gluon plasmas. *Rep. Prog. Phys.* **72,** 126001 (2009).
4. Inguscio, M., Ketterle, W. & Salomon, C. (eds) *Ultracold Fermi Gases* (Proc. Int. School of Physics 'Enrico Fermi', Course CLXIV, IOS, 2008).
5. O'Hara, K. M., Hemmer, S. L., Gehm, M. E., Granade, S. R. & Thomas, J. E. Observation of a strongly interacting degenerate Fermi gas of atoms. *Science* **298,** 2179–2182 (2002).
6. Riedl, S. *et al.* Collective oscillations of a Fermi gas in the unitarity limit: temperature effects and the role of pair correlations. *Phys. Rev. A* **78,** 053609 (2008).
7. Cao, C. *et al.* Universal quantum viscosity in a unitary Fermi gas. *Science* **331,** 58–61 (2011).
8. Enss, T., Haussmann, R. & Zwerger, W. Viscosity and scale invariance in the unitary Fermi gas. *Ann. Phys.* **326,** 770–796 (2011).
9. Jo, G.-B. *et al.* Itinerant ferromagnetism in a Fermi gas of ultracold atoms. *Science* **325,** 1521–1524 (2009).
10. Stringari, S. Density and spin response function of a normal Fermi gas at unitarity. *Phys. Rev. Lett.* **102,** 110406 (2009).
11. Duine, R. A., Polini, M., Stoof, H. T. C. & Vignale, G. Spin drag in an ultracold Fermi gas on the verge of ferromagnetic instability. *Phys. Rev. Lett.* **104,** 220403 (2010).
12. D'Amico, I. & Vignale, G. Theory of spin Coulomb drag in spin-polarized transport. *Phys. Rev. B* **62,** 4853–4857 (2000).
13. Weber, C. P. *et al.* Observation of spin Coulomb drag in a two-dimensional electron gas. *Nature* **437,** 1330–1333 (2005).
14. D'Amico, I. & Vignale, G. Coulomb interaction effects in spin-polarized transport. *Phys. Rev. B* **65,** 085109 (2002).
15. Gedik, N., Orenstein, J., Liang, R., Bonn, D. A. & Hardy, W. N. Diffusion of nonequilibrium quasi-particles in a cuprate superconductor. *Science* **300,** 1410–1412 (2003).
16. Garwin, R. L. & Reich, H. A. Self-diffusion and nuclear relaxation in $He^3$. *Phys. Rev.* **115,** 1478–1492 (1959).
17. Anderson, A. C., Edwards, D. O., Roach, W. R., Sarwinski, R. E. & Wheatley, J. C. Thermal and magnetic properties of dilute solutions of $He^3$ in $He^4$ at low temperatures. *Phys. Rev. Lett.* **17,** 367–372 (1966).
18. DeMarco, B. & Jin, D. S. Spin excitations in a Fermi gas of atoms. *Phys. Rev. Lett.* **88,** 040405 (2002).
19. Du, X., Luo, L., Clancy, B. & Thomas, J. E. Observation of anomalous spin segregation in a trapped Fermi gas. *Phys. Rev. Lett.* **101,** 150401 (2008).
20. Zwierlein, M. W., Schirotzek, A., Schunck, C. H. & Ketterle, W. Fermionic superfluidity with imbalanced spin populations. *Science* **311,** 492–496 (2006).
21. Shin, Y., Zwierlein, M., Schunck, C., Schirotzek, A. & Ketterle, W. Observation of phase separation in a strongly interacting imbalanced Fermi gas. *Phys. Rev. Lett.* **97,** 030401 (2006).
22. Vichi, L. & Stringari, S. Collective oscillations of an interacting trapped Fermi gas. *Phys. Rev. A* **60,** 4734–4737 (1999).
23. Nascimbène, S., Navon, N., Jiang, K. J., Chevy, F. & Salomon, C. Exploring the thermodynamics of a universal Fermi gas. *Nature* **463,** 1057–1060 (2010).
24. Bruun, G. M., Recati, A., Petchick, C. J., Smith, H. & Stringari, S. Collisional properties of a polarized Fermi gas with resonant interactions. *Phys. Rev. Lett.* **100,** 240406 (2008).
25. Bruun, G. M. Spin diffusion in Fermi gases. *New J. Phys.* **13,** 035005 (2011).
26. Polini, M. & Vignale, G. Spin drag and spin-charge separation in cold Fermi gases. *Phys. Rev. Lett.* **98,** 266403 (2007).
27. Parish, M. M. & Huse, D. A. Evaporative depolarization and spin transport in a unitary trapped Fermi gas. *Phys. Rev. A* **80,** 063605 (2009).
28. Gaebler, J. P. *et al.* Observation of pseudogap behavior in a strongly interacting Fermi gas. *Nature Phys.* **6,** 569–573 (2010).
29. Perali, A. *et al.* Evolution of the normal state of a strongly interacting Fermi gas from a pseudogap phase to a molecular Bose gas. *Phys. Rev. Lett.* **106,** 060402 (2011).
30. Partridge, G. B., Li, W., Kamar, R. I., Liao, Y. & Hulet, R. G. Pairing and phase separation in a polarized Fermi gas. *Science* **311,** 503–505 (2006).
31. Nascimbène, S. *et al.* Collective oscillations of an imbalanced Fermi gas: axial compression modes and polaron effective mass. *Phys. Rev. Lett.* **103,** 170402 (2009).
32. Ku, M. *et al.* Equation of state of a strongly interacting atomic Fermi gas. *Bull. Am. Phys. Soc.* **55,** abstr. W6. 00001 (2010); available at ⟨http://meetings.aps.org/link/BAPS.2010.DAMOP.W6.1⟩ (2010).


**Supplementary Information** is linked to the online version of the paper at www.nature.com/nature.

**Acknowledgements** We thank G. Bruun, C. Pethick, D. Huse, R. Duine and W. Zwerger for discussions, and A. Schirotzek for help with the early stages of the experiment. This work was supported by the NSF, AFOSR-MURI, ARO-MURI, ONR, DARPA YFA, a grant from the Army Research Office with funding from the DARPA OLE programme, the David and Lucille Packard Foundation and the Alfred P. Sloan Foundation.

**Author Contributions** All authors contributed to the experimental work. A.S. analysed the data. M.K. developed the algorithm for thermometry. M.W.Z. performed theoretical calculations. A.S. and M.W.Z wrote the manuscript.

**Author Information** Reprints and permissions information is available at www.nature.com/reprints. The authors declare no competing financial interests. Readers are welcome to comment on the online version of this article at www.nature.com/nature. Correspondence and requests for materials should be addressed to A.S. (atsommer@mit.edu).